

1 Dissolved Nitrogen Cycling in The Eastern Canadian Arctic Archipelago and Baffin Bay from  
2 Stable Isotopic Data

3 **H.C. Westbrook<sup>1</sup>, A. Bourbonnais<sup>1,\*</sup>, C.C.M. Manning<sup>2</sup>, J.-É. Tremblay<sup>3</sup>, M. M. M.**  
4 **Ahmed<sup>4</sup>, B. Else<sup>4</sup>, and J. Granger<sup>2</sup>**

5 <sup>1</sup> School of the Earth, Ocean and Environment, University of South Carolina, Columbia, SC,  
6 United States

7 <sup>2</sup> Department of Marine Sciences, University of Connecticut, Groton, Connecticut, United States

8 <sup>3</sup> Québec-Océan and Takuvik, Département de biologie, Université Laval, Québec, Québec,  
9 Canada

10 <sup>4</sup> Department of Geography, University of Calgary, Calgary, Alberta, Canada

11

12

13 Corresponding author: Annie Bourbonnais (abourbonnais@seoe.sc.edu)

14 **Key Points:**

15

- 16
- Nitrate in regional rivers derived proximately from nitrification.
  - Dissolved organic nitrogen concentrations in regional rivers were low.
  - Dissolved organic nitrogen consumption was observed in the ECAA and Baffin Bay with highest chlorophyll-a.
- 18
- 19
- 20

## 21 Abstract

22 Climate change is expected to alter the input of nitrogen (N) sources in the Eastern Canadian  
23 Arctic Archipelago (ECAA) and Baffin Bay due to increased discharge from glacial meltwater  
24 and permafrost thaw. Since dissolved inorganic N is generally depleted in surface waters,  
25 dissolved organic N (DON) could represent a significant N source fueling phytoplankton activity  
26 in Arctic ecosystems. Yet, few DON data for this region exist. We measured concentrations and  
27 stable isotope ratios ( $\delta^{15}\text{N}$  and  $\delta^{18}\text{O}$ ) of DON and nitrate ( $\text{NO}_3^-$ ) to investigate the sources and  
28 cycling of dissolved nitrogen in regional rivers and at the sea surface from samples collected in  
29 the ECAA and Baffin Bay during the summer of 2019. The isotopic signatures of  $\text{NO}_3^-$  in rivers  
30 could be reproduced in a steady state isotopic model by invoking mixing between atmospheric  
31  $\text{NO}_3^-$  and nitrified ammonium as well as  $\text{NO}_3^-$  assimilation by phytoplankton. DON  
32 concentrations were low in most rivers ( $\leq 4.9 \mu\text{mol L}^{-1}$ ), whereas the concentrations ( $0.54\text{--}12$   
33  $\mu\text{mol L}^{-1}$ ) and  $\delta^{15}\text{N}$  of DON ( $-0.71\text{--}9.6 \text{‰}$ ) at the sea surface were variable among stations,  
34 suggesting dynamic cycling and/or distinctive sources. In two regions with high chl-a, DON  
35 concentrations were inversely correlated with chlorophyll-a and the  $\delta^{15}\text{N}$  of DON, suggesting net  
36 DON consumption in localized phytoplankton blooms. We derived an isotope effect of  $-6.9\text{‰}$   
37 for DON consumption. Our data helps establish a baseline to assess future change in nutrient  
38 regime for this climate sensitive region.

## 39 Plain Language Summary

40 Primary productivity in the Arctic Ocean surface waters is limited by nitrogen supply. We  
41 investigated dissolved inorganic and organic nitrogen dynamics in the Eastern Canadian Arctic  
42 Archipelago (ECAA) and Baffin Bay surface ocean waters as well as adjacent rivers. We used  
43 the isotopic composition (N and O) of both dissolved organic and inorganic nitrogen (DON and  
44 DIN, respectively) to explore the sources and transformations of nitrogen. Nitrate in rivers was  
45 from both from the atmosphere and from nitrified ammonium. Nitrate was also consumed by  
46 phytoplankton. DON concentrations were low in rivers compared to inorganic nitrogen (i.e.,  
47 nitrate). This observation contrast with previous data collected in the Eurasian and U.S. western  
48 coastal Arctic Ocean, where rivers input a high quantity of DON to the coastal ocean. We  
49 observed variable DON concentrations and isotopic composition in the ECAA and Baffin Bay  
50 surface ocean waters, suggesting different sources and/or a dynamic DON cycling. We  
51 additionally found evidence for DON consumption in regions of highest chlorophyll-a. These  
52 data are important to better understand how Greenland's melting ice sheet will impact nutrient  
53 delivery and primary productivity in the region.

## 54 Introduction

55 Climate change is rapidly altering Arctic ecosystems. As air and seawater temperatures  
56 are rising, sea ice volume is decreasing and seasonal river discharge is increasing (Wu et al.,  
57 2005; Wassmann et al., 2011; Bintanja & Selten, 2014; Feng et al., 2021). The critical roles  
58 played by the Arctic Ocean in controlling the thermohaline circulation and supporting fisheries  
59 (Link & Tol, 2009) have stimulated scientific research in the region within the past few decades.  
60 While primary productivity is expected to increase for most Arctic shelves, similar changes are  
61 not ubiquitous across the entire Arctic (Arrigo et al., 2015; Lewis et al., 2020). For example,  
62 decreased nutrient delivery through physical circulation as well as increased stratification due to  
63 higher freshwater input may decrease primary productivity overall in the Canada Basin and the  
64 Eastern Canadian Arctic Archipelago (ECAA), including Baffin Bay, the Nares Strait, Lancaster

65 Sound, and Jones Sound (McLaughlin & Carmack, 2010; Lehmann et al., 2019). Nutrients in the  
66 surface waters of the ECAA are typically low unless there are localized sources, such as rivers  
67 and inputs from glacially-driven upwelling (Tank et al., 2012; Thibodeau et al., 2017; Cape et  
68 al., 2019; Bhatia et al., 2022). The availability of nutrients, as well as access to sunlight, are the  
69 key factors controlling primary productivity in the western Arctic basins (Tremblay et al., 2015).  
70 Nitrogen is ultimately limiting in the western Arctic (Tremblay et al., 2006; Yamamoto-Kawai et  
71 al., 2006) and thus sources and sinks of nitrogen need to be constrained to better understand the  
72 current N budget as a baseline to assess future changes.

73 The ECAA is fed predominantly by Pacific generated water from the Canada Basin  
74 moving eastward and exiting at Lancaster Sound. Arctic water also enters through Nares Strait,  
75 carrying Pacific water and underlying Atlantic-origin water. In Baffin Bay, Arctic water mixes  
76 with underlying Atlantic water directly from the North Atlantic via the West Greenland current.  
77 Additionally, freshwater is introduced into the ECAA from river and glacial melt as the coastline  
78 of the region is peppered with glaciers and has high permafrost coverage. Based on  
79 stoichiometric nutrient tracers and nitrate isotope ratios ( $\delta^{15}\text{N}$ ), nutrients are dominantly from  
80 Pacific-derived water, albeit mixed with Atlantic-derived waters supplying about 25% of the  
81 nitrate ( $\text{NO}_3^-$ ) (Lehmann et al., 2022, and references therein).

82 Dissolved organic nitrogen (DON) typically accounts for the largest pool of dissolved  
83 nitrogen in freshwater and marine surface waters (Sipler & Bronk, 2014). Although dominated  
84 by refractory species, the labile fraction of DON can be an essential source of N to primary  
85 producers, especially in N limited regions (Bronk et al., 2007; Moschonas et al., 2017;  
86 Thibodeau et al., 2017; Knapp et al., 2018). DON is composed of a highly refractory pool, and a  
87 smaller labile pool, such as amino acids or DNA, which can be utilized on time scales ranging  
88 from hours to years. DON can be produced *in situ* in the oceans through mechanisms such as the  
89 viral lysing of bacteria or the loss of prey biomass during feeding by microzooplankton (Sipler &  
90 Bronk, 2014). Rivers are one of the major DON sources to the ocean due to the presence of  
91 terrestrial organic matter. As a result, DON tends to be higher in coastal areas than in the open  
92 ocean, although the utilization of DON is not limited to coastal regions. DON can be produced  
93 by surface plankton in productive areas and then transported out into N limited regions, fueling  
94 primary productivity (Letscher et al., 2013; Knapp et al., 2018; Bif et al., 2022).

95 The Arctic Ocean is heavily impacted by rivers, receiving 10% of global river discharge  
96 despite accounting for only 4% of the global ocean surface (Wu et al., 2005; Holmes et al.,  
97 2012). River runoff, permafrost thaw and coastal erosion are significant sources of nutrients in  
98 Arctic coastal regions (Tank et al., 2012; Le Fouest., 2013; Treat et al., 2016; Thibodeau et al.,  
99 2017; Terhaar et al., 2021). Riverine input is typically high in areas such as the Laptev Sea and  
100 the western Arctic which are fed by large rivers. For example, the Lena River and the Mackenzie  
101 River have total dissolved nitrogen (TDN) concentrations around 15 to 20  $\mu\text{mol N L}^{-1}$  and  
102 discharge into the Laptev Sea and the Beaufort Sea, respectively. Dissolved inorganic N  
103 delivered by rivers is immediately consumed, as surface coastal Arctic waters are generally  
104 devoid of  $\text{NO}_3^-$  (Emmerton et al., 2008; Tremblay et al., 2014; Tremblay et al., 2015). The fate of  
105 riverine DON in coastal marine waters is still unclear, whether it is utilized, or simply diluted  
106 through mixing with DON-deplete waters. For instance, in the Arctic surface ocean, DON  
107 concentrations are on average 4.7  $\mu\text{mol N L}^{-1}$ , which is less than the concentrations in major  
108 Arctic rivers, which range from 7.4–18.4  $\mu\text{mol N L}^{-1}$  (Sipler & Bronk, 2014). Several studies  
109 support that riverine DON in the Arctic is slowly remineralized, representing a significant source

110 of bioavailable N to the open ocean. Tank et al. (2012) suggested that riverine  $\text{NO}_3^-$  and DON in  
 111 the coastal Laptev Sea region contribute to primary productivity, albeit for a relatively small  
 112 fraction (<10% each) of the overall Arctic Ocean primary production. Thibodeau et al. (2017)  
 113 found that DON concentrations discharged from the Lena River in the Eurasian Arctic were up  
 114 to six times higher than riverine  $\text{NO}_3^-$  concentrations and that DON was rapidly consumed  
 115 nearshore, with over 50% of it disappearing before reaching the shelf. However, Dittmar et al.  
 116 (2001) concluded that DON input from Siberian rivers did not substantially support primary  
 117 productivity, as it was largely recalcitrant. With riverine discharge increasing since around the  
 118 1960s (Peterson et al., 2002; Wu et al., 2005), the extent to which rivers influence the delivery of  
 119 bioavailable DON in Arctic coastal waters needs to be further investigated.

120 While previous studies have largely focused on the inputs of nutrient from large rivers in  
 121 past decades (e.g., Tank et al., 2012; Thibodeau et al., 2017), deliveries of  $\text{NO}_3^-$  and dissolved  
 122 organic nitrogen (DON) by small rivers and glacially-fed rivers (i.e. marine terminating glaciers  
 123 and glacial-fed rivers), and their impacts on coastal oceanic primary productivity in the ECAA  
 124 and Baffin Bay, has not been as thoroughly explored. Inputs of  $\text{NO}_3^-$  to surface waters was  
 125 shown to occur by upwelling induced by rising submarine glacial melt discharge in proximity to  
 126 the Greenland Ice Sheet and Jones Sound (Cape et al., 2019; Bhatia et al., 2021) and glacial melt  
 127 (Beaton et al., 2017). However, the input of exogenous DON to the surface ocean from glacial  
 128 melt has not been considered thus far. Upwelling regions generally see elevated DON  
 129 concentrations following the increase in biological activity due to  $\text{NO}_3^-$  input from below (Sipler  
 130 & Bronk, 2014). Since many rivers are of glacial origin in the ECAA and Baffin Bay, both  
 131 glacial and terrestrial riverine end members must be constrained in order to identify the sources  
 132 of DON in this rapidly changing region.

133 The naturally occurring stable N and O isotope ratios of dissolved N species can be  
 134 exploited to identify N sources and transformations in environmental samples. The nitrogen  $^{15}\text{N}$   
 135 / $^{14}\text{N}$  isotope ratios are reported in delta notation ( $\delta$ ) and units of per mil (‰), where the  $^{15}\text{N}/^{14}\text{N}$   
 136 and  $^{18}\text{O}/^{16}\text{O}$  references are atmospheric  $\text{N}_2$  for N and Vienna Standard Mean Ocean Water  
 137 (VSMOW) for O.

$$138 \quad \delta^{15}\text{N} = \left[ \left( \frac{^{15}\text{N}/^{14}\text{N}_{\text{sample}}}{^{15}\text{N}/^{14}\text{N}_{\text{air}}} \right) - 1 \right] \times 1000$$

$$139 \quad \delta^{18}\text{O} = \left[ \left( \frac{^{18}\text{O}/^{16}\text{O}_{\text{sample}}}{^{18}\text{O}/^{16}\text{O}_{\text{VSMOW}}} \right) - 1 \right] \times 1000$$

140 The  $\delta^{15}\text{N}$  of  $\text{NO}_3^-$  and DON is influenced originally by the  $\delta^{15}\text{N}$  of its source(s) and  
 141 secondarily by the fractionation imposed during phytoplankton uptake and DON decomposition  
 142 (see Knapp et al., 2005). The  $\delta^{15}\text{N}$  of  $\text{NO}_3^-$  and DON can thus be diagnostic of dominant sources  
 143 of new N in a system. The DON produced by  $\text{N}_2$ -fixing organisms as well as newly nitrified  
 144  $\text{NO}_3^-$  from this source are expected to reflect the low  $\delta^{15}\text{N}$  of newly fixed ammonium ( $\text{NH}_4^+$ ; -2  
 145 to 0‰) (Minagawa & Wada, 1986; Carpenter et al., 1997; Knapp et al., 2018) or N from  
 146 atmospheric deposition with a similarly low  $\delta^{15}\text{N}$  (Altieri et al., 2016 and references therein).  
 147 Conversely, the  $\delta^{15}\text{N}$  DON released by phytoplankton is more elevated, reflecting the  $\delta^{15}\text{N}$  of the  
 148 incident inorganic N substrates. The  $\delta^{15}\text{N}$  of nitrate varies regionally, posting a global ocean  
 149 average of 5‰, but the  $\delta^{15}\text{N}$  of Pacific waters of western Arctic basins is distinctly higher at 8‰  
 150 (Knapp et al., 2005; Knapp et al., 2018). DON and  $\text{NO}_3^-$  produced through newly regenerated N,  
 151 typically  $\text{NH}_4^+$ , will often have a lower  $\delta^{15}\text{N}$  compared to ambient substrate pools as lighter  
 152 isotopes are preferentially excreted (Fawcett et al., 2011).

153 In turn the  $\delta^{18}\text{O}$  of  $\text{NO}_3^-$  is distinct among N sources and also sensitive to  $\text{NO}_3^-$   
154 production and consumption terms. The  $\delta^{18}\text{O}$  of  $\text{NO}_3^-$  in atmospheric deposition is exceptionally  
155 high (e.g., Hastings et al., 2003). Nitrate produced by the nitrification of ammonium empirically  
156 converges on  $\delta^{18}\text{O}$  of water. (Casciotti et al. 2010; Buchwald et al., 2012). Assimilatory and  
157 dissimilatory  $\text{NO}_3^-$  consumption results in a parallel increase of both  $\delta^{18}\text{O}$  and  $\delta^{15}\text{N}$  in a 1:1 ratio  
158 (Granger et al., 2004, 2008) in proportion to nitrate consumed. This relationship can be used to  
159 determine the influence of processes other than assimilation on the  $\text{NO}_3^-$  pool.

160 The goals of this study are to determine, using an isotopic approach, 1) the dominant  
161 sources of  $\text{NO}_3^-$  and DON in the ECAA and Baffin Bay and 2) the transformations affecting  
162 these pools. This study focuses on the Nares Strait, Jones Sound, Lancaster Sound, and Baffin  
163 Bay, whose coastal regions are more extensively bordered by glaciers compared to other Arctic  
164 regions. This region of the Arctic also experiences high permafrost coverage. Nutrient input from  
165 other sources, such as terrestrial rivers, are more significant in other Arctic regions such as the  
166 Laptev Sea and the western Arctic (Letscher et al., 2012; Thibodeau et al., 2017). The Eastern  
167 Baffin Bay is a highly productive area important for fisheries in Greenland. Determining the  
168 sources of nutrient inputs to coastal waters is essential to predict the effect of climate change on  
169 primary productivity in these economically important regions.

## 170 **2 Materials and Methods**

### 171 **2.1 Sample Location and Collection**

172 Samples were collected during Leg 2a and 2b of the ArcticNet expedition aboard the  
173 CCGS *Amundsen* from July 5<sup>th</sup> to August 15<sup>th</sup> of 2019. The expedition took place in the ECAA  
174 including Baffin Bay, the Nares Strait, Lancaster Sound, and Jones Sound. Sampling locations  
175 and regional circulation patterns are presented in Figure 1. In this region, prevailing currents  
176 flow southward through Nares Strait and into Kane Basin, Smith Sound, and finally Baffin Bay.  
177 Additionally, in northwestern Baffin Bay, currents flow eastward from Lancaster Sound into  
178 Baffin Bay. At the surface, these water masses are Pacific-derived and circulate in the Canadian  
179 and Makarov Basins before entering the ECAA through the Nares Strait and Lancaster Sound,  
180 respectively. In Baffin Bay, Atlantic water enters along the southwestern coast of Greenland and  
181 travels north until it converges with water flowing south from the Smith Sound and circulates  
182 southwards on the eastern side of Baffin Island (Lehmann 2019; 2022; Tang et al., 2004).  
183 Atlantic water from the Eurasian Basin of the Arctic Ocean can be found at depth in Baffin Bay  
184 (Alkire et al., 2010). Ice cover in this region varies by season and along an east-west gradient,  
185 with the lowest coverage in the summer and ice persisting much longer on the western side of  
186 Baffin Bay in spring (Tang et al., 2004). Some sea ice in Baffin Bay is formed locally, while  
187 some is formed in the Nares Strait and transported south. Ice formed in other channels is  
188 typically blocked by landfast ice and does not enter Baffin Bay (Tang et al., 2004).

189 Samples for DON analysis were collected using 12 L Niskin bottles at depths of 100 m  
190 and 80 m, and then upwards to the surface in 10 m intervals. Samples at 100 and 80 m were  
191 collected in 15 mL centrifuge tubes, and samples taken above 80 m were collected in 60 mL  
192 HDPE plastic bottles. All centrifuge tubes and bottles were acid-washed and rinsed three times  
193 with sample water prior to collection. All samples were frozen with a headspace to allow for  
194 water expansion upon freezing, until analysis. Samples taken during Leg 2b were also filtered  
195 with GF/F filters before freezing. Leg 2a samples were filtered prior to analysis with Supor<sup>TM</sup>  
196 0.45 micron polyethersulfone filters. A comparison was performed on the effect of the different

197 filters on [DON] and  $\delta^{15}\text{N}$  DON and no significant difference was observed. Riverine samples  
198 were collected from surface waters of 11 rivers, filtered with GF/F filters, and frozen. Water  
199 samples were also collected for  $\delta^{18}\text{O}$  of  $\text{H}_2\text{O}$  analysis; samples were collected without bubbles in  
200 2 mL glass vials and stored at  $4^\circ\text{C}$ .

## 201 **2.2 Concentration and Isotopic Analysis of DON, $\text{NO}_3^-$ , and $\delta^{18}\text{O}$ of $\text{H}_2\text{O}$**

202 The concentration and  $\delta^{15}\text{N}$  of DON were measured as in Knapp et al. (2005). Briefly,  
203 total dissolved nitrogen (TDN) was oxidized to  $\text{NO}_3^-$  using recrystallized persulfate followed by  
204 measurement on a  $\text{NO}_x$  analyzer by chemiluminescent detection (Braman & Hendrix, 1989). An  
205 unoxidized sample was also used to measure dissolved inorganic nitrogen (DIN). [DON] was  
206 estimated as the difference between TDN and DIN. The  $\delta^{15}\text{N}$  of  $\text{NO}_3^-$  was then analyzed using  
207 the denitrifier method (Sigman & Casciotti, 2001; Weigand et al., 2016).

208 As there is currently no efficient means to remove DIN, the combined concentration and  
209 isotopic composition of  $\text{NO}_3^-$  and  $\text{NO}_2^-$  (and  $\text{NH}_4^+$  if present) must be analyzed to calculate the  
210  $\delta^{15}\text{N}$  of DON by isotopic mass balance. [ $\text{NO}_3^- + \text{NO}_2^-$ ] was thus also measured by  
211 chemiluminescence prior to persulfate oxidation and the  $\delta^{15}\text{N}$  of  $\text{NO}_3^-$  only (i.e., without the  
212 persulfate oxidation step) was determined using the denitrifier method (Sigman & Casciotti,  
213 2001; Casciotti et al., 2002; Weigand et al., 2016).

214 [ $\text{NO}_3^-$ ], [ $\text{NO}_2^-$ ] and [ $\text{PO}_4^{3-}$ ] were also measured at sea using a nutrient autoanalyzer.  
215 Nitrite concentrations were generally below detection limit in our samples, with maximum  
216 values of  $1.3\ \mu\text{M}$  in marine samples and  $1.4\ \mu\text{M}$  in riverine samples. Only samples in which  
217 DON represents over 50% of TDN were considered. Ammonium in riverine samples was  
218 measured using a SEAL Nutrient Analyzer.

219 To prepare samples for TDN analysis, 1 mL of freshly prepared persulfate oxidizing  
220 reagent (POR) was added to 6 mL of sample in 12 mL threaded test tubes with Teflon-lined  
221 phenolic screw caps (Corning 99447-161). These samples were then autoclaved for one hour.  
222 POR blank was typically  $<0.4\ \mu\text{mol N L}^{-1}$  and [TDN] was corrected for blank contribution.  
223 Additionally,  $5\ \mu\text{mol N L}^{-1}$  of the international standards USGS-40, USGS-64, and USGS-65  
224 and an internal standard of 6-aminocaproic acid were analyzed with each run to verify oxidation  
225 efficiency and that no fractionation occurred during the persulfate oxidation step. The average  
226 percent yield of standard concentrations were  $>95\%$ , and the standard deviation from known  
227 isotopic composition was  $\pm 0.37\%$ .

228 Prior to isotopic analysis, the pH of autoclaved samples, standards, and blanks were  
229 adjusted to 3–4 with 6 N HCl. Neutralized samples were injected into 2 mL of *Pseudomonas*  
230 *chlororaphis* suspended in media. When analyzing  $\text{NO}_3^-$  alone, *Pseudomonas aureofaciens* was  
231 instead used to measure the  $\delta^{18}\text{O}$  of  $\text{NO}_3^-$ . In the few  $\text{NO}_3^-$  samples in which  $\text{NO}_2^-$  accumulated,  
232  $\text{NO}_2^-$  was removed using sulfamic acid as in Granger & Sigman, (2009). The target sample size  
233 was 20 nmol. The product  $\text{N}_2\text{O}$  was purified and analyzed using a continuous flow isotope ratio  
234 mass spectrometer (Elementar Americas PrecisiON) equipped with a custom on-line gas  
235 extraction and purge-trap system and PAL autosampler. Samples were standardized using a two-  
236 point correction with the international standards IAEA N-3 ( $\delta^{15}\text{N} = 4.7\%$  vs air) and USGS-34  
237 ( $\delta^{15}\text{N} = -1.8\%$  vs air). The  $\delta^{15}\text{N}$  of DON was determined by isotopic mass balance taking into  
238 consideration the concentration and  $\delta^{15}\text{N}$  of the POR blank as well as sample  $\text{NO}_3^-$  and TDN.  
239 The average standard deviation for duplicate  $\delta^{15}\text{N}$ -DON analysis was generally lower than  
240  $\pm 0.5\%$ . Error propagation was determined using a Monte Carlo method as in Knapp et al.  
241 (2018).

242 The  $\delta^{18}\text{O}$  of  $\text{H}_2\text{O}$  was measured using an integrated off-axis cavity absorption  
 243 spectrometer (Los Gatos Research, LGR, Triple Liquid Water Isotope Analyzer, model 912-  
 244 0032) at the University of Calgary as described in Ahmed et al. (2020). Chlorophyll-a was  
 245 measured using High Performance Liquid Chromatography (HPLC) at the University of British  
 246 Columbia as described in Burt et al. (2018). Plots of surface data and cross-sections were  
 247 generated with the Ocean Data View software (Schlitzer, 2021).

### 248 2.3 Mixing Model

249  $\delta^{18}\text{O}$  of  $\text{H}_2\text{O}$  and salinity were used in the following simple mixing model in order to  
 250 determine the relative contributions of marine water (*mar*), freshwater (*fw*), and sea ice melt  
 251 (*sim*).

$$\begin{aligned} 252 \quad & f_{mar} + f_{fw} + f_{sim} = 1 \\ 253 \quad & f_{mar} * S_{mar} + f_{fw} * S_{fw} + f_{sim} * S_{sim} = S_{measured} \\ 254 \quad & f_{mar} * O_{mar} + f_{fw} * O_{fw} + f_{sim} * O_{sim} = O_{measured} \end{aligned}$$

255 Wherein *f* is the fraction of each end member, *S* is salinity and *O* is  $\delta^{18}\text{O}$  of  $\text{H}_2\text{O}$ . End  
 256 member values used in the calculations are listed in Table 2.1. There are two important  
 257 freshwater sources in our system: rivers and glacial water. These two sources have identical  
 258 salinities (0) and overlapping  $\delta^{18}\text{O}$  of  $\text{H}_2\text{O}$  values,  $-17$  to  $-25\text{‰}$  for river water and  $-20.5$  to  
 259  $-21.7\text{‰}$  for glacial water (Bedard et al., 1981; Thibodeau et al., 2017; Brown et al., 2020;). Thus  
 260 we cannot distinguish between these end members with this dataset, and used a value of  $-20 \text{‰}$   
 261 for the freshwater  $\delta^{18}\text{O}$  end member. The contribution of sea ice melt can be considered in two  
 262 regards: as net sea ice melt or local sea ice melt. Net sea ice melt is integrated over time and  
 263 reflects the difference between ice formation during the winter and ice melt during the spring and  
 264 summer. Local sea ice melt is the instantaneous contribution of sea ice melt at the time of  
 265 sampling. In both cases, a positive value indicates melting, and a negative value indicates  
 266 formation. Because the melting and formation of sea ice are decoupled in time and space, the  
 267 contribution of sea ice melt determined from the end members in Table 2.1 represents net sea ice  
 268 melt rather than local sea ice melt, and local sea ice melt is not determined in this study.

269 Additionally, because this region has marine water originating from both the Pacific and  
 270 Atlantic Oceans, we first determine the fraction of Pacific ( $f_{PW}$ ) and Atlantic water ( $f_{AW}$ ) in a  
 271 given sample, assuming that  $f_{PW} + f_{AW} = 1$  (Jones et al., 1998; Yamamoto-Kawai et al., 2008;  
 272 Sherwood et al., 2021; Lehmann et al. 2022). We utilize  $N^*$ , a semi conservative nutrient tracer  
 273 based on the amount of excess DIN relative to phosphate assuming Redfield stoichiometry (i.e.,  
 274 16N:1P) to determine  $f_{PW}$  and  $f_{AW}$ . We calculate the  $N^*$  of a sample using the equation below, and  
 275 presume that nitrate is not affected by benthic denitrification in the CAA, a supposition that  
 276 appears valid (Lehmann et al., 2022).

$$277 \quad N^* = (NO_3^- - 16 \times [PO_4^{3-}]) + 2.9$$

278 After  $N^*$  was calculated, we calculated  $f_{PW}$  in a given sample using the following  
 279 equation, wherein  $N^*_{PW} = -11 \mu\text{M}$ ,  $N^*_{AW} = 2.8 \mu\text{M}$ , and negative  $f_{PW}$  values indicate no Pacific  
 280 water contribution and were set to zero.

$$281 \quad f_{PW} = \frac{N^*_{sample} - N^*_{AW}}{N^*_{PW} - N^*_{AW}}$$

282 Finally, we adjust our marine endmember mixing model values ( $S_{\text{mar}}$  and  $O_{\text{mar}}$ ) based on  
 283 the fraction of Pacific and Atlantic water in the sample. Endmember values for Pacific and  
 284 Atlantic waters are provided in Table 1.

## 285 **2.4 Model for Riverine $\text{NO}_3^-$ Cycling**

286 A simple steady-state isotopic model was used to apportion the sources and sinks of  $\text{NO}_3^-$   
 287 in ECAA and Baffin Bay rivers. This model included two sources of  $\text{NO}_3^-$  supplied to rivers: 1)  
 288  $\text{NO}_3^-$  from the nitrification of  $\text{NH}_4^+$ , which may derive proximately from permafrost,  
 289 atmospheric  $\text{NH}_4^+$ , or in-river mineralization (e.g., Wagner et al., 2002; Alves et al., 2013;  
 290 Fouché et al., 2020) and 2) uncycled  $\text{NO}_3^-$  from atmospheric deposition (e.g., Hastings et al.,  
 291 2004). We assumed that complete nitrification of  $\text{NH}_4^+$  results in  $\text{NO}_3^-$  with a  $\delta^{15}\text{N}$  of  $\sim 1.2\text{‰}$   
 292 akin to atmospheric and permafrost end-members (range:  $-6$  to  $10\text{‰}$ ; (Wynn et al., 2007; Ansari  
 293 et al., 2013; Louiseize et al., 2014; Heikoop et al., 2015; Arendt et al., 2016; Clark et al., 2020).  
 294 The  $\delta^{18}\text{O}$  produced during the nitrification of  $\text{NH}_4^+$  was estimated to be  $\sim -14.2\text{‰}$  (range:  $-8.9$   
 295 to  $-19.5\text{‰}$ ), assuming that at least 2/3 of the O atoms are derived from water during nitrification  
 296 (Casciotti et al., 2010; Heikoop et al., 2015; Boshers et al., 2019). For this estimation, we assume  
 297 the  $\delta^{18}\text{O}$  of water ranges from  $-12\text{‰}$  to  $-22\text{‰}$  (Wynn et al., 2007; Arendt et al., 2016) and that  
 298  $\delta^{18}\text{O}$  of dissolved oxygen range from  $23.7\text{‰}$  to  $24.2\text{‰}$  based on the  $\delta^{18}\text{O}$  of air (Horibe et al.,  
 299 1973; Kiddon et al., 1993; Wang & Veizer, 2000) as in Wynn et al., (2007). Additionally, we  
 300 assumed isotope effects on the  $\delta^{18}\text{O}$   $\text{NO}_3^-$  and exchange with  $\text{H}_2\text{O}$  during bacterial nitrification  
 301 as in Casciotti et al. (2010) and Buchwald et al. (2012). We also assumed that  $\text{NH}_4^+$  was  
 302 completely oxidized to  $\text{NO}_3^-$  in rivers, as  $\text{NH}_4^+$  was absent or very low in all our samples, with  
 303 the highest concentration being  $0.56\text{ }\mu\text{M}$  at R-ESC. We assumed that atmospheric deposition  
 304 added  $\text{NO}_3^-$  with a  $\delta^{15}\text{N}$  of  $-3.5\text{‰}$  and a  $\delta^{18}\text{O}$  of  $72.1\text{‰}$  (Hastings et al., 2004; Ansari et al.,  
 305 2013; Louiseize et al., 2014; Heikoop et al., 2015). We assumed an kinetic N isotope effect ( $\epsilon$ ) of  
 306  $5\text{‰}$  for  $\text{NO}_3^-$  assimilation (Altabet, 2001) and a corresponding  $^{18}\epsilon:^{15}\epsilon$  of 1:1 (Granger et al.,  
 307 2004). The isotope effect is defined as  $^{15}\epsilon = ((^{14}k/^{15}k) - 1) \times 1000$ , where  $^{14}k$  and  $^{15}k$  are the rate  
 308 coefficients of the reactions for the light and heavy isotopes respectively. We excluded  
 309 denitrification, the canonical conversion of  $\text{NO}_3^-$  to the nitrogen gases  $\text{N}_2\text{O}$  and  $\text{N}_2$  under  
 310 anaerobic conditions, due to the high  $\text{O}_2$  concentrations in the rivers (Dalsgaard et al., 2014). We  
 311 considered two main scenarios for the extent of N recycling and its impact on primary  
 312 production within the rivers: 1) 50% recycled production, and 2) 25% recycled production. More  
 313 details about the model are included in the Supporting Information.

314 We used this model to reproduce the deviation from the  $^{18}\epsilon:^{15}\epsilon$  ratio of  $\sim 1$  observed for  
 315 pure  $\text{NO}_3^-$  assimilation (Granger et al., 2004) of our riverine samples. We refer to this deviation  
 316 as the  $\Delta(15,18)$ , which is the difference between  $\text{NO}_3^-$   $\delta^{15}\text{N}$  and  $\delta^{18}\text{O}$  (Rafter et al., 2013).

## 317 **2.5 Isotope Effect of DON Consumption**

318 In areas where chlorophyll-a was the highest, we estimated the  $^{15}\epsilon$  of DON consumption  
 319 using a closed system Rayleigh model ( $\delta^{15}\text{N}$  of DON vs  $\ln([\text{DON}])$ ) as in Knapp et al. (2018). A  
 320 low  $[\text{DON}]$  concomitant with elevated  $\delta^{15}\text{N}$  indicates consumption, as kinetic isotope  
 321 fractionation during consumption increases the  $\delta^{15}\text{N}$  of the residual DON pool.

## 322 3 Results

### 323 3.1 Physical Characteristics of the ECAA and Baffin Bay

324 Near shore waters were influenced by freshwater input from rivers and/or glacial  
325 meltwater, as evidenced by fresher surface waters with distinctly low  $\delta^{18}\text{O}$   $\text{H}_2\text{O}$  values ( $-6.05$ –  
326  $0.54$ ‰), suggesting mixing with meteoric water (Mellat et al., 2021). This was evident throughout  
327 the study region, more distinct near Talbot Inlet, at the Petermann Glacier, at the Jakobshavn  
328 Glacier, in Lancaster Sound, and near the riverine stations R-SG and R-ESC in Jones Sound.  
329 (Figure 2). The fraction of freshwater and fraction of sea ice melt in surface waters of the study  
330 area are depicted in Figure 2 A&B, respectively. Stations closest to land had a higher fraction of  
331 freshwater, as expected. The low fraction of freshwater on the eastern coast of Transect 1 and 2 ( $0$   
332 to  $0.05$ ) observed in this study has been attributed to upwelling as well as influence from the West  
333 Greenland Current, which is more saline than the Baffin Current (Alkire et al., 2010). Sea ice melt  
334 was highest on the western side of Transect 2, which is close to the mouth of the Clyde River.

335 Many of the rivers sampled in this study were glacially fed, particularly those on Ellesmere  
336 Island such as R-ESG and R-6.1. Others were not located near glaciers, for example R-DIW and  
337 R-DIW-N on western Devon Island, and R-CP on Cornwallis. River ranged from  $0.5$  to  $3$  meters  
338 deep and  $\sim 1$  to  $\sim 30$  meters wide.  $\delta^{18}\text{O}$  of  $\text{H}_2\text{O}$  in rivers ranged from  $-18.4$  to  $-28.4$  ‰ (Brown et  
339 al., 2022).

### 340 3.2 Chlorophyll-a

341 Chlorophyll-a concentrations at the surface ( $4$  m) were low throughout the study region  
342 (typically  $< 2$   $\mu\text{g L}^{-1}$ ) except in the northern Nares Strait, where a particularly large bloom near  
343 Petermann Glacier was observed, as well as in Jones Sound, and the western side of Transect 1  
344 (Figure 3).

### 345 3.3 Nitrate Concentration and isotopic composition in the ECAA and Baffin Bay

346 Nitrate was near zero in all surface waters, except in the Jones sound, as well as the  
347 eastern and western ends of the Davis Strait (Transect 1 in Figure 1, Figure 4). At Transect 1 the  
348  $\delta^{15}\text{N}$  of  $\text{NO}_3^-$  was lower in the east ( $6.5$ ‰), and higher in the west ( $9.8$ ‰), where higher  
349 chlorophyll-a was also observed (Figure 3).  $\delta^{18}\text{O}$  of  $\text{NO}_3^-$  across this transect was similar in the  
350 east ( $3.3$ ‰) and west ( $3.4$ ‰). Additionally at the mouth of Jones sound, a  $\delta^{15}\text{N}$  and  $\delta^{18}\text{O}$  of  $\text{NO}_3^-$   
351 of  $14$ ‰ and  $50$ ‰ were observed. Nitrate was generally completely consumed in the mixed layer  
352 (upper  $10$  m) within the study area and increased with depth to up to  $\sim 15$   $\mu\text{M}$  at  $100$  m depth  
353 (Figure S2).

354 Nitrate concentration and isotopic composition of river samples are provided in Table 2.  
355 The concentration of  $\text{NO}_3^-$  among riverine samples covered a broad range, from  $0.44$  to  $47$   $\mu\text{M}$ ,  
356 (Table 2). Nitrite was  $< 0.2$   $\mu\text{M}$  in all samples, both riverine and marine, except for R-6.1, which  
357 had  $1.4$   $\mu\text{M}$   $\text{NO}_2^-$ . High variability was observed even in rivers adjacent to one another, such as  
358 R-6.1 and R-ESG. The isotopic composition of  $\text{NO}_3^-$  was highly variable between rivers,  
359 indicating variability in  $\text{NO}_3^-$  sources and/or transformations among these Arctic rivers. R-SG  
360 had the lowest  $\delta^{15}\text{N}$  of  $\text{NO}_3^-$  ( $0.71$ ‰) and a  $\text{NO}_3^-$  concentration of  $2.7$   $\mu\text{M}$ . R-ESG had the  
361 highest  $\delta^{15}\text{N}$  of  $\text{NO}_3^-$  ( $10.3$ ‰) and a  $\text{NO}_3^-$  concentration of  $0.44$   $\mu\text{M}$ . The adjacent river R-6.1  
362 had a similarly elevated  $\delta^{15}\text{N}$  of  $\text{NO}_3^-$  of  $10$ ‰ but much higher  $\text{NO}_3^-$  concentration of  $11$   $\mu\text{M}$ .  
363 The river at R-6.1 was about  $20$ – $30$  meters wide. In contrast, R-ESG was a river running through

364 a crevasse adjacent to Eugenie Glacier and was only ~1 meter wide. R-ESG and R-6.1 were  
 365 drastically different with respect to their  $\delta^{18}\text{O}$  of  $\text{NO}_3^-$ , which was  $-2.7\text{‰}$  in R-6.1 and  $49\text{‰}$  in  
 366 R-ESG.

367 High variation was also observed between R-ESC and R-SG, both of which are west of  
 368 Grise Fjord. R-SG was around 5 meters wide and ~0.5 meters deep, while R-ESC was roughly  
 369 20 meters wide and 1–2 meters deep. Additionally, R-ESC was more inland than R-SG. R-SG  
 370 and R-ESC had similar  $\text{NO}_3^-$  concentrations, but the  $\delta^{15}\text{N}$  of  $\text{NO}_3^-$  was almost  $2\text{‰}$  higher at R-  
 371 ESC than R-SG. Furthermore, the  $\delta^{18}\text{O}$  of  $\text{NO}_3^-$  at R-ESC was nearly 4.5 times lower than that at  
 372 R-SG. Conversely, two other stations in similar areas, R-DIW and R-DIW-N, both located on the  
 373 west side of Devon Island had significantly different  $\text{NO}_3^-$  concentrations ( $20\ \mu\text{M}$  and  $47\ \mu\text{M}$ ,  
 374 respectively), but similar isotopic signatures ( $4.4\text{‰}$  &  $4.8\text{‰}$ , respectively).

375 We consider that the isotopic composition of riverine  $\text{NO}_3^-$  derived from two end-  
 376 member sources, namely  $\text{NO}_3^-$  produced proximately by nitrification and uncycled atmospheric  
 377  $\text{NO}_3^-$ . However, the  $\text{NO}_3^-$  isotopic composition of our samples did not fall along the mixing line  
 378 for the two end members. The isotope values were potentially explained by also invoking the  
 379 partial assimilation of  $\text{NO}_3^-$  and associated isotopic enrichment of residual  $\text{NO}_3^-$  (Figure 5). This  
 380 indicates that atmospheric depositions, assimilation and nitrification contributed, to some extent,  
 381 to the  $\delta^{15}\text{N}$  and  $\delta^{18}\text{O}$  of  $\text{NO}_3^-$  signatures of the river samples.

382 Additionally, we used a steady-state isotopic model to confirm that these 3 processes  
 383 (nitrification, atmospheric depositions and  $\text{NO}_3^-$  assimilation) could produce the deviation from  
 384 the  $^{18}\text{O}:^{15}\text{N}$  ratio of ~1 observed for pure  $\text{NO}_3^-$  assimilation (Granger et al., 2004) for our riverine  
 385 samples. We define the deviation from the  $^{18}\text{O}:^{15}\text{N}$  ratio of ~1 as the difference between  $\text{NO}_3^-$   $\delta^{15}\text{N}$   
 386 and  $\delta^{18}\text{O}$ , referred to as  $\Delta(15,18)$  (Rafters et al., 2013). Assuming that 25% of the dissolved  
 387 nitrogen was recycled within the rivers, we were able to reproduce the full range of observed  
 388  $\Delta(15,18)$  (Figure 6).

### 389 **3.4 DON Distribution and $\delta^{15}\text{N}$ in the ECAA and Baffin Bay**

390 The surface distribution of DON concentrations and the  $\delta^{15}\text{N}$  of DON are shown in  
 391 Figure 7. DON concentrations were highly variable but had similar values between regions,  
 392 ranging from  $3.2$  to  $6.1\ \mu\text{mol N L}^{-1}$  in Baffin Bay and  $3.2$  to  $6.0\ \mu\text{mol N L}^{-1}$  in the Nares Strait.  
 393 Lancaster Sound and Jones Sound had lower DON concentrations, ranging from  $2.1$  to  $5.7\ \mu\text{mol}$   
 394  $\text{N L}^{-1}$ . In the mixed layer (upper 10 meters) of the water column, [DON] increased with salinity  
 395 (Figure 8). This suggests a low [DON] freshwater end member, corroborating our direct riverine  
 396 measurements of [DON] (mean  $1.7 \pm 1.5\ \mu\text{M NL}^{-1}$ ). [DON] in riverine samples were moderate-  
 397 to-low ( $0 - 4.9\ \mu\text{M NL}^{-1}$ ), even when  $\text{NO}_3^-$  was high.

398 Yet, no significant relationship between [DON] and the fraction of freshwater input was  
 399 observed in Jones Sound, where the highest freshwater fraction was observed (Figure 2A).  
 400 [DON] also fell above or below the pure mixing line at other stations, suggesting surface ocean  
 401 DON production and consumption processes (Figure 8). The relationship between DON  
 402 concentration and  $\delta^{15}\text{N}$  with depth was variable and often only characterized within the upper 40  
 403 m because  $\text{NO}_3^-$  concentrations below 40 m depth were often too high to allow calculating the  
 404  $\delta^{15}\text{N}$  of DON from isotopic mass balance. Concentration and  $\delta^{15}\text{N}$  of DON increased with depth  
 405 in Transects 1 & 2, Lancaster Sound, and in some areas near Disko Island. DON trends with  
 406 depth in the Nares Strait were variable. The depth relationship between [DON] and  $\delta^{15}\text{N}$  was

407 more variable at some of the more southernmost stations, which either showed an increase in  
408 [DON] associated with a slight decrease in  $\delta^{15}\text{N}$ , a slight increase in both  $\delta^{15}\text{N}$  and [DON] or no  
409 change in isotopic composition. The higher [DON] observed for the eastern sections of both  
410 transects could have been caused by Ekman-driven upwelling, which is supported by salinity  
411 profiles (Figure S1).

412 In two areas where highest chlorophyll-a concentrations were measured, the Northern  
413 Nares Strait and Western Transect 1, chlorophyll-a and DON concentrations in the upper 10  
414 meters were inversely correlated Pearson  $R^2=0.75$  and p-value = 0.04, Spearman  $\rho=-1$  and  
415  $\ln([\text{DON}])$  and  $\delta^{15}\text{N}$ -DON were also inversely correlated (Pearson  $R^2 = 0.54$ , p-value = 0.10,  
416 Spearman  $\rho=-1$  and p-value = 0.02; Figure 10) in these regions. These trends were not observed  
417 in Jones Sound, where relatively high chlorophyll-a concentrations were also observed. No  
418 relationships were observed between the freshwater fraction and [DON] or freshwater fraction  
419 and  $\delta^{15}\text{N}$  of DON in Northern Nares Strait and Western Transect 1, precluding a significant  
420 source of low [DON] and elevated  $\delta^{15}\text{N}$  DON from rivers at these locations.

421

## 422 **4 Discussion**

### 423 **4.1 Deciphering $\text{NO}_3^-$ sources in the ECAA and Baffin Bay**

424 Nitrate was close to zero in the surface mixed layer at most stations (<10 m depth),  
425 though some surface stations had over 1  $\mu\text{M}$   $\text{NO}_3^-$  (Figure 4). While some of the rivers sampled  
426 had upwards of 10  $\mu\text{M}$   $\text{NO}_3^-$ , these elevated concentrations were not observed in coastal marine  
427 waters. These data suggest that  $\text{NO}_3^-$  from the rivers was rapidly consumed or diluted along the  
428 coasts. Previous studies of riverine nutrients in the Arctic have similarly found that riverine  $\text{NO}_3^-$   
429 delivered into coastal Arctic waters was rapidly consumed nearshore (Emmerton et al., 2008;  
430 Tremblay et al., 2014; Tremblay et al., 2015). Riverine nutrient input can increase productivity  
431 locally in some near-shore regions, but this only represents a relatively minor fraction of net  
432 marine primary productivity in the Arctic (Tremblay et al., 2015). While few blooms were  
433 identified through discrete chlorophyll-a sampling, satellite data for July and August 2019 in this  
434 region show higher chlorophyll-a nearshore (Figure S4).

435 The concentration and isotopic composition of riverine  $\text{NO}_3^-$  were highly variable  
436 spatially, indicating variable contributions of end-member sources, and production and  
437 consumption terms. We considered two main sources of  $\text{NO}_3^-$  in rivers: atmospheric deposition  
438 or the proximate nitrification of  $\text{NH}_4^+$  from either permafrost or atmospheric deposition (and  
439 internal recycling). Some rivers with low [ $\text{NO}_3^-$ ] had particularly high  $\delta^{18}\text{O}$ , up to 48‰,  
440 suggesting a significant fraction of uncycled atmospheric  $\text{NO}_3^-$ . The  $\delta^{18}\text{O}$  of  $\text{NO}_3^-$  from  
441 atmospheric deposition in the summer reflects the  $\delta^{18}\text{O}$  of the O sources, which are ozone ( $\text{O}_3$ )  
442 and hydroxyl radicals (OH).  $\text{O}_3$  has a higher  $\delta^{18}\text{O}$  (90–122‰; (Krankowsky et al., 1995;  
443 Johnston & Thiemens, 1997), while OH usually has  $\delta^{18}\text{O} < 0$  (Hastings et al., 2004).  $\text{NO}_3^-$   
444 receives two O atoms from  $\text{O}_3$ , and one from OH, significantly increasing the  $\delta^{18}\text{O}$  of  $\text{NO}_3^-$  from  
445 atmospheric deposition (65.2 to 79.6‰; Hastings et al., 2004). Additionally, other rivers had a  
446 low  $\delta^{18}\text{O}$  of  $\text{NO}_3^-$  (7 out of 11 rivers with  $\delta^{18}\text{O}$  of  $\text{NO}_3^- < 0$ ‰), which portends of nitrification of  
447 exogenous and recycled  $\text{NH}_4^+$ . During nitrification, most of the O atoms originate from water,  
448 hence the  $\delta^{18}\text{O}$  of newly nitrified  $\text{NO}_3^-$  approaches the O isotopic signature of its  $\text{H}_2\text{O}$  source  
449 (Boshers et al., 2019). Since freshwater in high latitude systems has a lower  $\delta^{18}\text{O}$  of  $\text{H}_2\text{O}$

450 (~-22‰; (Louiseize et al., 2014; Arendt et al., 2016), the lower  $\delta^{18}\text{O}$  of  $\text{NO}_3^-$  observed in some  
451 ECAA river waters could indicate a significant input from nitrification.

452 To determine the contribution of these end members we used a steady-state isotopic  
453 model described in section 2.4 and the supporting information, and were able to reproduce the  
454 range of observed  $\delta^{15}\text{N}$ ,  $\delta^{18}\text{O}$  as well as  $\Delta(15,18)$  in riverine samples (Figure 6). The  $\text{NO}_3^-$   
455 isotopic signatures (both  $\delta^{15}\text{N}$  and  $\delta^{18}\text{O}$ ) suggested that mixing between atmospheric  $\text{NO}_3^-$  and  
456 nitrified  $\text{NH}_4^+$  alone could not account for the observed  $\delta^{15}\text{N}$  and  $\delta^{18}\text{O}$ . However, including  
457  $\text{NO}_3^-$  assimilation helped explain the observed dual  $\text{NO}_3^-$  isotopic values (solid arrow in Figure  
458 5). This requirement for  $\text{NO}_3^-$  removal by assimilation is corroborated by previous studies, which  
459 have observed the uptake of  $\text{NO}_3^-$  by phytoplankton in Arctic rivers (Snyder & Bowden, 2014;  
460 Beaton et al., 2017). Our isotopic model also suggests that the majority of our data appear to be  
461 more influenced by the input of microbially-derived (nitrified)  $\text{NO}_3^-$  rather than uncycled  
462 atmospheric  $\text{NO}_3^-$ . This indicates that nitrification is putatively an important process to provide  
463 bioavailable N to Arctic rivers. Some Canadian Arctic permafrost is known to have a large  
464 quantity of  $\text{NH}_4^+$  (Fouché et al., 2020), and contact with permafrost can influence the chemical  
465 composition of rivers (Frey et al., 2007; Frey & McClelland, 2009; Heikoop et al., 2015; Vonk et  
466 al., 2015). Additionally,  $\text{NH}_4^+$  can be found in atmospheric deposition in similar proportions to  
467 atmospheric  $\text{NO}_3^-$  (Clark et al., 2020; Fouché et al., 2020). Moreover,  $\text{NO}_3^-$  input from  
468 atmospheric deposition appears to be temporally variable. In the Canadian Arctic, atmospheric  
469 deposition can be a dominant source of  $\text{NO}_3^-$  in rivers during the early melt season, which was  
470 from early June to mid-July. Rivers in this study were sampled after this melt season, during  
471 which remineralization takes over as the dominant source of  $\text{NO}_3^-$  (Louiseize et al., 2014).  
472 Though nitrification of  $\text{NH}_4^+$  derived from permafrost or atmospheric deposition was the  
473 predominant source of  $\text{NO}_3^-$  (or recycling), some rivers had significantly higher  $\text{NO}_3^-$   
474 concentrations and varying isotopic compositions, even when located geographically in close  
475 proximity to one another. For instance, rivers R-6.1 ( $[\text{NO}_3^-] = 11 \mu\text{M}$ ) and R-ESG ( $[\text{NO}_3^-] =$   
476  $0.44 \mu\text{M}$ ) were adjacent and both had a  $\delta^{15}\text{N}$  of 10‰, but R-ESG had the lowest  $\Delta(15,18)$   
477 (-38‰) and the highest  $\delta^{18}\text{O}$  of  $\text{NO}_3^-$  (49‰). In contrast, R-6.1 had a relatively high  $\Delta(15,18)$   
478 (13‰), and a lower  $\delta^{18}\text{O}$  of  $\text{NO}_3^-$  (-2.7‰). We attribute this extreme variability to different  
479 landscape features associated with these rivers. R-ESG was running directly through a glacier,  
480 while R-6.1 was next to a glacial moraine containing significant terrestrial material. Therefore,  
481 R-ESG was likely in more direct contact with the glacial end member than R-6.1 and thus might  
482 have a relatively higher atmospherically-derived  $\text{NO}_3^-$  fraction. We posit that the sources of  
483 nitrogen in these rivers greatly vary depending on watershed characteristics and microbial  
484 metabolisms as suggested by Kaiser et al. (2017), even within small spatial scales.

#### 485 **4.2 DON mixing and transformations in the ECAA and Baffin Bay**

486 Several factors control primary productivity in the Arctic, including nitrogen, iron and  
487 light availability (Tremblay et al., 2015). Ongoing Arctic sea-ice loss is expected to increase  
488 light availability, and drastically impact primary productivity and, consequently biological  $\text{CO}_2$   
489 intake (Arrigo, 2007; Frey, 2018; Hill et al., 2018). Furthermore, river discharges from Arctic  
490 watersheds are steadily increasing in response to changes in the North Atlantic Oscillation and  
491 global mean surface air temperature (Peterson et al., 2002; McClelland et al., 2016; Rood et al.,  
492 2017). These rivers transport massive quantities of dissolved and particulate inorganic and  
493 organic nitrogen, sustaining primary productivity in coastal waters (Letscher, et al., 2013;  
494 McClelland et al., 2016; Thibodeau et al., 2017). Conversely, increased river discharge and

495 coastal erosion can lead to unfavorable nearshore light conditions, which could negatively  
496 impact primary productivity (Terhaar et al., 2021).

497 In this study,  $\text{NO}_3^-$  concentrations were extremely low (maximum of  $1.3 \mu\text{M}$ ) or zero in  
498 the ECAA and Baffin Bay surface waters, which is consistent with N being the limiting nutrient  
499 in Arctic regions (Figure 4). However, DON accumulated to concentrations up to  $6.1 \mu\text{mol N L}^{-1}$   
500 in surface waters near Davis Strait (Figure 7A) and could thus sustain primary productivity if a  
501 significant fraction of that DON is labile. However, the labile versus recalcitrant DON fractions  
502 were not analyzed in this study.

503 The large differences in both concentrations and isotopic compositions observed in this  
504 study could be due to local variations in DON sources. Previous studies have found that the  $\delta^{15}\text{N}$   
505 of DON can reflect the  $\delta^{15}\text{N}$  of the new N source (Knapp et al., 2018). Therefore, DON produced  
506 from a low  $\delta^{15}\text{N}$  source, such as newly nitrified  $\text{NO}_3^-$  from  $\text{N}_2$  fixation, can have a similarly low  
507  $\delta^{15}\text{N}$  DON. In samples where we were able to measure both  $\delta^{15}\text{N}$  of  $\text{NO}_3^-$  and DON, the  $\delta^{15}\text{N}$  of  
508 DON was on average  $\sim 4 \text{‰}$  lower than that of  $\text{NO}_3^-$  which could indicate DON production from  
509  $\text{NO}_3^-$ . Knapp et al. (2018) observed a similar trend in the Eastern Tropical South Pacific surface  
510 waters, where subsurface DON bracketed the  $\delta^{15}\text{N}$  of  $\text{NO}_3^-$  by  $\pm 3 \text{‰}$ . Additionally, the lack of  
511 variation in DON isotopic composition and concentration observed in some areas, such as  
512 Transect 4, where  $[\text{DON}]$  ranged from  $5.7\text{--}6.1 \mu\text{mol N L}^{-1}$  and  $\delta^{15}\text{N}$ –DON ranged from  $4.8\text{--}$   
513  $4.9 \text{‰}$ , could suggest recalcitrant DON (Knapp et al., 2005; Bourbonnais et al., 2009).

514 Previous studies suggest that rivers are generally a significant source of bioavailable  
515 DON. For instance, Lobbes et al. (2000) reported an average  $[\text{DON}]$  of  $12 \mu\text{M}$  for several  
516 Russian rivers. Conversely, Thibodeau et al. (2017) measured DON concentrations ranging  
517 between  $13.9$  to  $21.8 \mu\text{M}$  in the Siberian Arctic. These studies found that up to 70% of the  
518 terrigenous DON delivered by Arctic rivers was consumed within the shelf waters of the western  
519 and Eurasian Arctic (Letscher et al., 2013; Thibodeau et al., 2017). Our results contrast with  
520 findings from other Arctic regions, such as the Siberian and Western Arctic (Lobbes et al., 2000;  
521 Dittmar et al., 2001; Holmes et al., 2012; Thibodeau et al., 2017). Rivers measured in this study  
522 generally had relatively high  $\text{NO}_3^-$  but were mostly depleted in DON (up to  $4.9 \mu\text{mol N L}^{-1}$  in R-  
523 ESG). Our study thus suggests that rivers in the ECAA and Baffin Bay could act to dilute the  
524 DON pool in adjacent coastal marine surface waters. Overall,  $[\text{DON}]$  seemed to decrease with  
525 salinity in the mixed surface layer (upper 10 meters), though this correlation was overall not  
526 significant (Figure 8). Increased freshwater inputs with low DON concentrations could further  
527 stratify the water column in coastal ECAA and Baffin Bay waters, inhibiting vertical exchange  
528 with nutrient-rich deep waters, potentially decreasing primary productivity in the region if DIN is  
529 concomitantly low. The differences in DON concentrations observed between studies are likely  
530 related to the amount of glacial coverage, as the ECAA and Baffin Bay have significantly higher  
531 glacial coverage than the western and Eurasian Arctic (Pfeffer et al., 2014).

532 DON concentrations reported for glacial rivers are greatly variable. For example, on the  
533 Greenland Ice Sheet and the Leverett Glacier, which is adjacent to eastern Transect 1, previous  
534 studies reported a range from  $5.1\text{--}14 \mu\text{M}$  for DON in the surface ice, while DON in basal ice and  
535 summer ice melt was on average about  $12 \mu\text{M}$  and  $3.0 \mu\text{M}$ , respectively (Wadham et al., 2016;  
536 Holland et al., 2019). The higher DON values in both locations were attributed to the presence of  
537 debris or microbial production of DON. However, other studies reported near zero DON  
538 concentration in supraglacial streams, cryoconite melt water, snow, and short ice cores (Telling  
539 et al., 2012; Wadham et al., 2016; Holland et al., 2019). In contrast, runoff from the Leverett

540 Glacier had an average DON concentration of 1.7  $\mu\text{M}$ , with a maximum of 6.3  $\mu\text{M}$  (Wadham et  
541 al., 2016). This average value is low relative to the average [DON] of the adjacent marine waters  
542 ( $5.6 \mu\text{mol N L}^{-1}$ ). Thus, the low [DON] seen in river samples in this study could be  
543 characteristic of glacial melt that has not significantly mixed with high DON basal ice or debris.

544 Notably, Western Lancaster Sound, where a particularly high fraction of freshwater was  
545 observed, is fed by several rivers which we directly sampled. The rivers R-DIW, R-DIW-N, and  
546 R-CP all drain into western Lancaster Sound and had low [DON], ranging from 0.99–2.2  $\mu\text{mol N}$   
547  $\text{L}^{-1}$ . This is a lower concentration than the surface ocean [DON] of this region, which is  $\sim 4 \mu\text{mol}$   
548  $\text{N L}^{-1}$  but more similar to the [DON] in run off from the Leverett Glacier in the Greenland ice  
549 sheet (0.1–6.3  $\mu\text{M}$ , mean of 1.7  $\mu\text{M}$ ; Wadham et al., 2016). All the [DON] values of rivers in this  
550 study fall within this range, though none of these rivers were draining from the Greenland Ice  
551 Sheet. While this can be viewed as a localized input of nutrients, at a larger scale this serves to  
552 both stratify and dilute the nearshore nitrogen pool. Thus, our direct measurements of [DON] in  
553 Arctic rivers corroborate dilution of the marine DON pool by riverine freshwater. Deviations  
554 from a pure mixing line in Figure 8 strongly suggest that competing sources or transformations  
555 are affecting the DON pool, e.g., inputs from freshwater and buoyancy or Ekman-driven  
556 upwellings and *in-situ* production/consumption by phytoplankton assemblages in the mixed  
557 surface waters (Thibodeau et al., 2017; Cape et al., 2019; Bhatia et al., 2022). The DON pool  
558 would also be influenced by the lability of the localized sources.

559 Our isotopic model for riverine  $\text{NO}_3^-$  suggested that nitrified  $\text{NH}_4^+$  was a significant  
560 source of  $\text{NO}_3^-$  in most rivers observed in this study. However, rivers in direct contact with  
561 organic matter sources such as permafrost and debris are typically DON-rich (Frey et al., 2007;  
562 Frey & McClelland, 2009; Wadham et al., 2016; Fouché et al., 2020). These contrasting  
563 observations suggest that most of the  $\text{NO}_3^-$  in rivers in this study could be atmospherically  
564 derived (either from nitrification of  $\text{NH}_4^+$  or direct  $\text{NO}_3^-$  inputs). Future studies should better  
565 constrain the isotopic composition ( $\delta^{15}\text{N}$ ) and lability of permafrost DON, as well as soil  
566 conditions which can affect nitrogen cycling. For example, Frey & McClelland (2007) suggest  
567 that organic nitrogen in the permafrost of Alaskan watersheds was more easily remineralized  
568 compared to West Siberian watersheds, as the Siberian watersheds have high water saturation,  
569 which can limit remineralization of DON and facilitate denitrification. Due to analytical  
570 limitations, we were unable to analyze  $\delta^{15}\text{N}$ -DON in all but two of our riverine samples.  
571 Improvements to the analytical methods for measuring stable isotopes of DON (e.g., capability to  
572 remove DIN prior to DON analysis) could elucidate the contribution of permafrost in delivering  
573 DON to glacially fed rivers.

574 Both R-SG and R-ESG had slightly elevated  $\delta^{15}\text{N}$ -DON (5.8‰ and 7.2‰, respectively).  
575 Prior studies have observed low  $\delta^{15}\text{N}$ -DON in rivers and streams, at around  $-4$  to 2‰  
576 (Thibodeau et al., 2017; Ye et al., 2018). These values have been attributed to N sources from  
577 atmospheric deposition, aquatic and/or terrestrial  $\text{N}_2$  fixation, or plant litter decomposition.  
578 Assuming DON sources in these rivers would have similar  $\delta^{15}\text{N}$  to this range, the values  
579 observed here could be considered elevated, and may indicate kinetic isotope fractionation  
580 during consumption or a source of recalcitrant DON with a particularly high  $\delta^{15}\text{N}$ . DON  
581 consumption will preferentially utilize the lighter isotopes, elevating the  $\delta^{15}\text{N}$ -DON of the  
582 remaining pool (e.g., Knapp et al., 2005; Bourbonnais et al., 2009; Knapp et al., 2018).  
583 Identifying the sources and lability of DON in these rivers, and the microbial processes involved

584 could provide further insights on how changes in river discharge and glacial coverage will affect  
585 DON supply.

586 Sea ice melt represents another potential source of DON in the ECAA and Baffin Bay.  
587 Similar to surface ice in some glaciers, sea ice can have higher concentration of DON, as  
588 observed in the Antarctic (Fripiat et al., 2014; Dall'Osto et al., 2017). Fripiat et al. (2014)  
589 suggested high DON was released by microbial communities within the sea ice following  $\text{NO}_3^-$   
590 assimilation. However, no significant correlation was observed between sea ice melt and DON in  
591 this study. Higher resolution sea ice melt and DON datasets, as well as direct measurements of  
592 DON in Arctic sea ice could help explore this potential contribution.

### 593 **4.3 Evidence for DON consumption**

594 DON consumption was identified at two main regions in the study area. One of the  
595 signals of DON consumption is isotopic enrichment of the DON pool (Knapp et al., 2018).  
596 During consumption,  $^{14}\text{N}$  is preferentially taken up, resulting in an increase in the  $\delta^{15}\text{N}$  of the  
597 substrate in surface waters. We observed a negative relationship between chlorophyll-a and DON  
598 concentrations in both the northern segment of the Nares Strait and the western half of Transect 1  
599 (Pearson  $R^2 = 0.75$ , p-value = 0.04, Spearman  $\rho = -1$ , p-value = 0.02; Figure 9). Though Jones  
600 sound also has high chlorophyll, we have excluded it in this analysis as we suspect riverine  
601 discharge (Figure S3) is obscuring the relationship between chlorophyll-a, DON, and  $\delta^{15}\text{N}$  of  
602 DON. Additionally, [DON] was negatively correlated with  $\delta^{15}\text{N}$  (Pearson  $R^2 = 0.54$ , p-value =  
603 0.10, Spearman  $\rho = -1$ , p-value = 0.02) (Figure 10). Our derived isotope effect of  $-6.9\%$  using a  
604 closed-system Rayleigh model, is comparable to previously measured isotope effects of DON  
605 consumption of  $-5.5\%$  (Knapp et al., 2018).

606 We observe that higher chlorophyll-a is correlated with lower [DON], which contrasts  
607 with the relationship found by Knapp et al. (2018). Knapp et al. (2018) observed a positive  
608 correlation between surface ocean chlorophyll-a and DON concentrations in the eastern tropical  
609 South Pacific, consistent with a photosynthetic source for DON. Conversely, nutrient  
610 concentration has been shown to decrease as chlorophyll-a increases due to nutrient uptake by  
611 phytoplankton in incubation studies (Cruz et al., 2006; Buapet et al., 2008), and a similar inverse  
612 relationship has been observed between DON and chlorophyll-a in lakes (Berman, 1997). We  
613 posit that the low DON associated with high chlorophyll-a observed here is the result of net  
614 DON uptake by phytoplankton.

615 Though [DON] remains at around  $4\text{--}5 \mu\text{M N L}^{-1}$  in the surface waters throughout most  
616 of the study region and  $\text{NO}_3^-$  is near or at zero, we do not observe a distinct consumption signal  
617 at other stations. Several possibilities could explain this observation. First, any correlation  
618 between [DON] and chlorophyll-a is likely hindered by the low spatial resolution of available  
619 chlorophyll-a measurements, though satellite data corroborates our observations of mostly low  
620 chlorophyll-a in Baffin Bay (Figure S4). Second, DON could be recalcitrant in some regions.  
621 Dittmar et al. (2001) found that DON in the Siberian Arctic in brackish mixing zones was  
622 relatively recalcitrant. Third, DON cycling is likely complex and highly dynamic, with  
623 simultaneous consumption and production decoupled in space and time. These processes could  
624 complicate the relationship between chlorophyll-a and DON.

## 625 5 Conclusions

626 Nitrogen is a limiting nutrient in the ECAA and Baffin Bay, but its cycling and dynamics  
627 are not well constrained, particularly with regards to DON. As river discharges are projected to  
628 increase under a warmer climate, it is critical to better understand the role of glacial rivers in  
629 delivering nitrogen to this climate sensitive region.

630  $\text{NO}_3^-$  was the dominant dissolved nitrogen species in rivers. Our stable isotopic data  
631 suggests that a significant fraction of this  $\text{NO}_3^-$  was assimilated in the river and/or rapidly  
632 consumed near shore. Thus, while increased river discharge may increase riverine  $\text{NO}_3^-$  flux, the  
633 impact on primary productivity may be limited to coastal regions (Tank et al., 2012; Tremblay et  
634 al., 2015). We used a steady-state isotopic box model to apportion the sources of  $\text{NO}_3^-$  in rivers.  
635 Our model suggested that  $\text{NO}_3^-$  assimilation in addition to mixing between inputs from  
636 atmospheric deposition and nitrified  $\text{NH}_4^+$  is needed to explain the observed  $\delta^{15}\text{N}$  and  $\delta^{18}\text{O}$  of  
637  $\text{NO}_3^-$  in rivers.  $\text{NO}_3^-$  putatively derived from the nitrification of permafrost or atmospheric  $\text{NH}_4^+$   
638 was found to be a main source of  $\text{NO}_3^-$  in most rivers, while only few rivers (e.g., R-ESG) had  
639 significant input of  $\text{NO}_3^-$  from atmospheric deposition.

640 DON concentrations were relatively low in rivers (less than  $4.9 \mu\text{mol N L}^{-1}$ ). Unlike  
641 relationships observed for coastal waters adjacent to major Arctic rivers (Letscher et al., 2013;  
642 Tremblay et al., 2014; Thibodeau et al., 2017), we observed that DON concentrations were  
643 generally increasing with salinity. We posit that increased riverine discharge in the ECAA and  
644 Baffin Bay may result in increased stratification of the surface ocean and dilution of the ambient  
645 DON pool, with potential effect on chlorophyll-a. However, it is important to note that  
646 geochemical signatures of Arctic rivers can vary seasonally (Alkire et al., 2017; Manning et al.,  
647 2020), and our river measurements were collected during a relatively narrow period (July 8<sup>th</sup> to  
648 August 14<sup>th</sup>, 2019) occurring after the peak annual discharge. Thus, the trends we observed may  
649 not be reflective of other times of the year. The low DON concentrations observed in the river  
650 contrast with those observed in large terrestrial rivers with extensive watersheds, such as the  
651 Mackenzie or Lena Rivers. We observed evidence for DON consumption (i.e., negative  
652 correlations between chlorophyll-a and  $\delta^{15}\text{N}$ -DON and DON concentrations) in the northern  
653 Nares Strait, as well as western Transect 1. This indicates that DON could be utilized by  
654 phytoplankton in the ECAA and Baffin Bay, although the source of this DON, as well as its  
655 composition and lability require further investigation. We estimated an isotope effect for DON  
656 consumption of  $-6.9\text{‰}$ , which is in line with previous studies ( $-5.5\text{‰}$ ; Knapp et al., 2018). This  
657 study provides a baseline for DON cycling in the ECAA and Baffin Bay and highlights further  
658 areas of research needed to better understand N-cycling in this dynamic region.

## 659 Acknowledgments, Samples, and Data

660 This work was funded by the National Science Foundation (NSF) (award #1927755 to  
661 Bourbonnais). Research on the CCGS Amundsen was funded by ArcticNet, a Network of  
662 Centres of Excellence Canada and the Amundsen Science program, which is supported through  
663 Université Laval by the Canada Foundation for Innovation. Data have been submitted to the NSF  
664 Arctic Data Center. Additionally, we thank Dr. Nadine Lehmann for providing the R code used  
665 for the Figure 1. Sample collection took place off the shores and within the rivers of Inuit,  
666 Inughuit Nunaat, and Kalaallit Nunaat land, and samples were analyzed on Congaree and  
667 Tsalaguwetiye land. We thank the crew of the CCGS Amundsen for making this research

668 possible. We also thank Darcy Perin, Maggie Gaspar, Elise Lumsden, Adrianna Webb, Jaquan  
669 High, and Miles Hampton for assistance in sample analysis.

## 670 References

- 671 Ahmed, M. M. M., Else, B. G. T., Capelle, D., Miller, L. A., & Papakyriakou, T. (2020).  
672 Underestimation of surface pCO<sub>2</sub> and air-sea CO<sub>2</sub> fluxes due to freshwater stratification in an  
673 Arctic shelf sea, Hudson Bay. *Elementa: Science of the Anthropocene*, 8(1).  
674 <https://doi.org/10.1525/elementa.084>
- 675 Alkire, M. B., Falkner, K. K., Boyd, T., & Macdonald, R. W. (2010). Sea ice melt and meteoric  
676 water distributions in Nares Strait, Baffin Bay, and the Canadian Arctic Archipelago. *Journal*  
677 *of Marine Research*, 68(6), 767–798. <https://doi.org/10.1357/002224010796673867>
- 678 Alkire, M. B., Jacobson, A. D., Lehn, G. O., Macdonald, R. W., & Rossi, M. W. (2017). On the  
679 geochemical heterogeneity of rivers draining into the straits and channels of the Canadian  
680 Arctic Archipelago. *Journal of Geophysical Research: Biogeosciences*, 122(10), 2527–2547.  
681 <https://doi.org/10.1002/2016jg003723>
- 682 Altabet, M. A. (2001). Nitrogen isotopic evidence for micronutrient control of fractional NO<sub>3</sub><sup>-</sup>  
683 utilization in the equatorial Pacific. *Limnology and Oceanography*, 46(2), 368–380.
- 684 Altieri, K. E., Fawcett, S. E., Peters, A. J., Sigman, D. M. & Hastings, M. G. Marine biogenic  
685 source of atmospheric organic nitrogen in the subtropical North Atlantic. *Proc National Acad*  
686 *Sci* 113, 925–930 (2016).
- 687 Alves, R. J. E., Wanek, W., Zappe, A., Richter, A., Svenning, M. M., Schleper, C., & Urich, T.  
688 (2013). Nitrification rates in Arctic soils are associated with functionally distinct populations  
689 of ammonia-oxidizing archaea. *The ISME Journal*, 7(8), 1620–1631.  
690 <https://doi.org/10.1038/ismej.2013.35>
- 691 Ansari, A. H., Hodson, A. J., Heaton, T. H. E., Kaiser, J., & Marca-Bell, A. (2013). Stable  
692 isotopic evidence for nitrification and denitrification in a High Arctic glacial ecosystem.  
693 *Biogeochemistry*, 113(1–3), 341–357. <https://doi.org/10.1007/s10533-012-9761-9>
- 694 Arendt, C. A., Heikoop, J. M., Newman, B. D., Wilson, C. J., Graham, D. E., Dafflon, B., et al.  
695 (2016). Isotopic and Chemical Identification of Hydrological Pathways in a Watershed  
696 Underlain by Shallow Discontinuous Permafrost, 2016, GC43E–1199.
- 697 Arrigo, K. (2007). Physical control of primary productivity in Arctic and Antarctic polynyas.  
698 *Elsevier Oceanography Series*, 74, 223–238.
- 699 Beaton, A. D., Wadham, J. L., Hawkings, J., Bagshaw, E. A., Lamarche-Gagnon, G., Mowlem,  
700 M. C., & Tranter, M. (2017). High-Resolution in Situ Measurement of Nitrate in Runoff from  
701 the Greenland Ice Sheet. *Environmental Science & Technology*, 51(21), 12518–12527.  
702 <https://doi.org/10.1021/acs.est.7b03121>
- 703 Bedard, P., Hillaire-Marcel, C., & Page, P. (1981). <sup>18</sup>O modelling of freshwater inputs in Baffin  
704 Bay and Canadian Arctic coastal waters. *Nature*, 293.
- 705 Berman, T. (1997). Dissolved organic nitrogen utilization by an Aphanizomenon bloom in Lake  
706 Kinneret. *Journal of Plankton Research*, 19(5), 577–586.
- 707 Bif, M. B. et al. Controls on surface distributions of dissolved organic carbon and nitrogen in the  
708 southeast Pacific Ocean. *Mar Chem* 244, 104136 (2022).
- 709 Bintanja, R., & Selten, F. M. (2014). Future increases in Arctic precipitation linked to local  
710 evaporation and sea-ice retreat. *Nature*, 509(7501), 479–482.  
711 <https://doi.org/10.1038/nature13259>

- 712 Bourbonnais, A., Lehmann, M. F., Waniek, J. J., & Schulz-Bull, D. E. (2009). Nitrate isotope  
713 anomalies reflect N<sub>2</sub> fixation in the Azores Front region (subtropical NE Atlantic). *Journal of*  
714 *Geophysical Research: Oceans (1978–2012)*, 114(C3). <https://doi.org/10.1029/2007jc004617>
- 715 Braman, R. S., & Hendrix, S. A. (1989). Nanogram Nitrite and Nitrate Determination in  
716 Environmental and Biological Materials by Vanadium(III) Reduction with  
717 Chemiluminescence Detection. *Analytical Chemistry*, 61, 2715–2718.
- 718 Brown, K. A. et al. Geochemistry of Small Canadian Arctic Rivers with Diverse Geological and  
719 Hydrological Settings. *J Geophys Res Biogeosciences* 125, (2020).
- 720 Brown, K. A., Manning, C. C. M., Jones, S. F., Izett, R. W., Capelle, D. W., Else, B. G. T., Eert,  
721 J., Tortell, P. D., McLennan, D., Peucker-Ehrenbrink, B., Williams, W. J. (2022): Canadian  
722 Arctic Archipelago Rivers Program: Nutrient, Dissolved Organic Carbon, and Water Isotope  
723 Data 2016-2019. PANGAEA, <https://doi.org/10.1594/PANGAEA.945702>, In: Brown, KA et  
724 al. (2022): *Canadian Arctic Archipelago Rivers Program: Geochemical Data 2016-2019*.  
725 PANGAEA, <https://doi.pangaea.de/10.1594/PANGAEA.945995> (dataset in review)
- 726 Buapet, P., Hiranpan, R., Ritchie, R. J., & Prathep, A. (2008). Effect of nutrient inputs on  
727 growth, chlorophyll, and tissue nutrient concentration of *Ulva reticulata* from a tropical  
728 habitat. *ScienceAsia*, 34(2), 245. <https://doi.org/10.2306/scienceasia1513-1874.2008.34.245>
- 729 Burt, W. J., Westberry, T. K., Behrenfeld, M. J., Zeng, C., Izett, R. W., & Tortell, P. D. (2018).  
730 Carbon: Chlorophyll Ratios and Net Primary Productivity of Subarctic Pacific Surface Waters  
731 Derived From Autonomous Shipboard Sensors. *Global Biogeochemical Cycles*, 32(2), 267–  
732 288. <https://doi.org/10.1002/2017gb005783>
- 733 Cape, M. R., Straneo, F., Beird, N., Bundy, R. M., & Charette, M. A. (2019). Nutrient release to  
734 oceans from buoyancy-driven upwelling at Greenland tidewater glaciers. *Nature Geoscience*,  
735 12(1), 34–39. <https://doi.org/10.1038/s41561-018-0268-4>
- 736 Casciotti, K L, Sigman, D. M., Hastings, M. G., Böhlke, J. K., & Hilkert, A. (2002).  
737 Measurement of the Oxygen Isotopic Composition of Nitrate in Seawater and Freshwater  
738 Using the Denitrifier Method. *Analytical Chemistry*, 74(19), 4905–4912.  
739 <https://doi.org/10.1021/ac020113w>
- 740 Casciotti, Karen L., McIlvin, M., & Buchwald, C. (2010). Oxygen isotopic exchange and  
741 fractionation during bacterial ammonia oxidation. *Limnology and Oceanography*, 55(2), 753–  
742 762. <https://doi.org/10.4319/lo.2010.55.2.0753>
- 743 Clark, S. C., Granger, J., Mastorakis, A., Aguilar-Islas, A., & Hastings, M. G. (2020). An  
744 Investigation into the Origin of Nitrate in Arctic Sea Ice. *Global Biogeochemical Cycles*,  
745 34(2). <https://doi.org/10.1029/2019gb006279>
- 746 Cruz, F. L.-D. la, Valenzuela-Espinoza, E., Millán-Núñez, R., Trees, C. C., Santamaría-del-  
747 Ángel, E., & Núñez-Cebrero, F. (2006). Nutrient uptake, chlorophyll-a and carbon fixation by  
748 *Rhodomonas* sp. (Cryptophyceae) cultured at different irradiance and nutrient concentrations.  
749 *Aquacultural Engineering*, 35(1), 51–60. <https://doi.org/10.1016/j.aquaeng.2005.08.004>
- 750 Dall’Osto, M., Ovadnevaite, J., Paglione, M., Beddows, D. C. S., Ceburnis, D., Cree, C., et al.  
751 (2017). Antarctic sea ice region as a source of biogenic organic nitrogen in aerosols. *Scientific*  
752 *Reports*, 7(1), 6047. <https://doi.org/10.1038/s41598-017-06188-x>
- 753 Dalsgaard, T., Stewart, F. J., Thamdrup, B., Brabandere, L. D., Revsbech, N. P., Ulloa, O., et al.  
754 (2014). Oxygen at Nanomolar Levels Reversibly Suppresses Process Rates and Gene  
755 Expression in Anammox and Denitrification in the Oxygen Minimum Zone off Northern  
756 Chile. *MBio*, 5(6), e01966-14. <https://doi.org/10.1128/mbio.01966-14>

- 757 Dittmar, T., Fitznar, H. P., & Kattner, G. (2001). Origin and biogeochemical cycling of organic  
758 nitrogen in the eastern Arctic Ocean as evident from D- and L-amino acids. *Geochimica et*  
759 *Cosmochimica Acta*, 65(22), 4103--4114.
- 760 Emmerton, C. A., Lesack, L. F. W., & Vincent, W. F. (2008). Nutrient and organic matter  
761 patterns across the Mackenzie River, estuary and shelf during the seasonal recession of sea-  
762 ice. *Journal of Marine Systems*, 74(3–4), 741–755.  
763 <https://doi.org/10.1016/j.jmarsys.2007.10.001>
- 764 Fawcett, S. E., Lomas, M. W., Casey, J. R., Ward, B. B., & Sigman, D. M. (2011). Assimilation  
765 of upwelled nitrate by small eukaryotes in the Sargasso Sea. *Nature Geoscience*, 4(10), 717–  
766 722. <https://doi.org/10.1038/ngeo1265>
- 767 Feng, D., Gleason, C.J., Lin, P. et al. Recent changes to Arctic river discharge. *Nat Commun* 12,  
768 6917 (2021)
- 769 Fouché, J., Christiansen, C. T., Lafrenière, M. J., Grogan, P., & Lamoureux, S. F. (2020).  
770 Canadian permafrost stores large pools of ammonium and optically distinct dissolved organic  
771 matter. *Nature Communications*, 11(1), 4500. <https://doi.org/10.1038/s41467-020-18331-w>
- 772 Frey, K. (2018). Arctic Ocean Primary Productivity: The Response of Marine Algae to Climate  
773 Warming and Sea Ice Decline. *Arctic Report Card 2018*, [https://www.Arctic.Noaa.](https://www.Arctic.Noaa.Gov/Report-Card/Report-Card-2018/ArtMID/7878/ArticleID/778/Arctic-Ocean-Primary-Productivity-The-Response-of-Marine-Algae-to-Climate-Warming-and-Sea-Ice-Decline)  
774 [Gov/Report-Card/Report-Card-2018/ArtMID/7878/ArticleID/778/Arctic-Ocean-Primary-](https://www.Arctic.Noaa.Gov/Report-Card/Report-Card-2018/ArtMID/7878/ArticleID/778/Arctic-Ocean-Primary-Productivity-The-Response-of-Marine-Algae-to-Climate-Warming-and-Sea-Ice-Decline)  
775 [Productivity-The-Response-of-Marine-Algae-to-Climate-Warming-and-Sea-Ice-Decline.](https://www.Arctic.Noaa.Gov/Report-Card/Report-Card-2018/ArtMID/7878/ArticleID/778/Arctic-Ocean-Primary-Productivity-The-Response-of-Marine-Algae-to-Climate-Warming-and-Sea-Ice-Decline)
- 776 Frey, K. E., & McClelland, J. W. (2009). Impacts of permafrost degradation on arctic river  
777 biogeochemistry. *Hydrological Processes*, 23(1), 169–182. <https://doi.org/10.1002/hyp.7196>
- 778 Frey, K. E., McClelland, J. W., Holmes, R. M., & Smith, L. C. (2007). Impacts of climate  
779 warming and permafrost thaw on the riverine transport of nitrogen and phosphorus to the  
780 Kara Sea. *Journal of Geophysical Research: Biogeosciences (2005–2012)*, 112(G4), n/a-n/a.  
781 <https://doi.org/10.1029/2006jg000369>
- 782 Fripiat, F., Sigman, D. M., Fawcett, S. E., Rafter, P. A., Weigand, M. A., & Tison, J. -L. (2014).  
783 New insights into sea ice nitrogen biogeochemical dynamics from the nitrogen isotopes.  
784 *Global Biogeochemical Cycles*, 28(2), 115–130. <https://doi.org/10.1002/2013gb004729>
- 785 Granger, J., & Sigman, D. M. (2009). Removal of nitrite with sulfamic acid for nitrate N and O  
786 isotope analysis with the denitrifier method. *Rapid Communications in Mass Spectrometry*,  
787 23(23), 3753–3762. <https://doi.org/10.1002/rcm.4307>
- 788 Granger, J., Sigman, D. M., Needoba, J. A., & Harrison, P. J. (2004). Coupled nitrogen and  
789 oxygen isotope fractionation of nitrate during assimilation by cultures of marine  
790 phytoplankton. *Limnology and Oceanography*, 49(5), 1763–1773.  
791 <https://doi.org/10.4319/lo.2004.49.5.1763>
- 792 Granger, J., Sigman, D. M., Gagnon, J., Tremblay, J., & Mucci, A. (2018). On the Properties of  
793 the Arctic Halocline and Deep Water Masses of the Canada Basin from Nitrate Isotope  
794 Ratios. *Journal of Geophysical Research: Oceans*, 123(8), 5443–5458.  
795 <https://doi.org/10.1029/2018jc014110>
- 796 Hastings, M. G., Steig, E. J., & Sigman, D. M. (2004). Seasonal variations in N and O isotopes  
797 of nitrate in snow at Summit, Greenland: Implications for the study of nitrate in snow and ice  
798 cores. *Journal of Geophysical Research: Atmospheres (1984–2012)*, 109(D20).  
799 <https://doi.org/10.1029/2004jd004991>
- 800 Heikoop, J. M., Throckmorton, H. M., Newman, B. D., Perkins, G. B., Iversen, C. M.,  
801 Chowdhury, T. R., et al. (2015). Isotopic identification of soil and permafrost nitrate sources

- 802 in an Arctic tundra ecosystem. *Journal of Geophysical Research: Biogeosciences*, 120(6),  
803 1000–1017. <https://doi.org/10.1002/2014jg002883>
- 804 Hill, V. J., Light, B., Steele, M., & Zimmerman, R. C. (2018). Light Availability and  
805 Phytoplankton Growth Beneath Arctic Sea Ice: Integrating Observations and Modeling.  
806 *Journal of Geophysical Research: Oceans*, 123(5), 3651–3667.  
807 <https://doi.org/10.1029/2017jc013617>
- 808 Holland, A. T., Williamson, C. J., Sgouridis, F., Tedstone, A. J., McCutcheon, J., Cook, J. M., et  
809 al. (2019). Dissolved organic nutrients dominate melting surface ice of the Dark Zone  
810 (Greenland Ice Sheet). *Biogeosciences*, 16(16), 3283–3296. [https://doi.org/10.5194/bg-16-](https://doi.org/10.5194/bg-16-3283-2019)  
811 [3283-2019](https://doi.org/10.5194/bg-16-3283-2019)
- 812 Holmes, R. M., McClelland, J. W., Peterson, B. J., Tank, S. E., Bulygina, E., Eglinton, T. I., et  
813 al. (2012). Seasonal and annual fluxes of nutrients and organic matter from large rivers to the  
814 Arctic Ocean and surrounding seas. *Estuaries and Coasts*, 35(2), 369--382.
- 815 Johnston, J. C., & Thiemens, M. H. (1997). The isotopic composition of tropospheric ozone in  
816 three environments. *Journal of Geophysical Research: Atmospheres*, 102(D21), 25395–  
817 25404. <https://doi.org/10.1029/97jd02075>
- 818 Kaiser, K., Canedo-Oropeza, M., McMahan, R., & Amon, R. M. W. (2017). Origins and  
819 transformations of dissolved organic matter in large Arctic rivers. *Scientific Reports*, 7(1),  
820 13064. <https://doi.org/10.1038/s41598-017-12729-1>
- 821 Kiddon, J., Bender, M. L., Orchardo, J., Caron, D. A., Goldman, J. C., & Dennett, M. (1993).  
822 Isotopic fractionation of oxygen by respiring marine organisms. *Global Biogeochemical*  
823 *Cycles*, 7(3), 679–694.
- 824 Knapp, A. N., Sigman, D. M., & Lipschultz, F. (2005). N isotopic composition of dissolved  
825 organic nitrogen and nitrate at the Bermuda Atlantic Time-series Study site. *Global*  
826 *Biogeochemical Cycles*, 19(1).
- 827 Knapp, A. N., Casciotti, K. L., & Prokopenko, M. G. (2018). Dissolved Organic Nitrogen  
828 Production and Consumption in Eastern Tropical South Pacific Surface Waters. *Global*  
829 *Biogeochemical Cycles*, 32(5), 769–783. <https://doi.org/10.1029/2017gb005875>
- 830 Knapp, A. N., Sigman, D. M., & Lipschultz, F. (2005). N isotopic composition of dissolved  
831 organic nitrogen and nitrate at the Bermuda Atlantic Time-series Study site. *Global*  
832 *Biogeochemical Cycles*, 19(1). <https://doi.org/10.1029/2004gb002320>
- 833 Krankowsky, D., Bartecki, F., Klees, G. G., Mauersberger, K., Schellenbach, K., & Stehr, J.  
834 (1995). Measurement of heavy isotope enrichment in tropospheric ozone. *Geophysical*  
835 *Research Letters*, 22(13), 1713–1716. <https://doi.org/10.1029/95gl01436>
- 836 Le Fouest, V., Babin, M. & Tremblay, J.-É. The fate of riverine nutrients on Arctic shelves.  
837 *Biogeosciences* 10, 3661–3677 (2013).
- 838 Lehmann, N., Kienast, M., Granger, J., Bourbonnais, A., Altabet, M. A., & Tremblay, J. -É.  
839 (2019). Remote Western Arctic Nutrients Fuel Remineralization in Deep Baffin Bay. *Global*  
840 *Biogeochemical Cycles*, 33(6), 649–667. <https://doi.org/10.1029/2018gb006134>
- 841 Lehmann, N., Kienast, M., Granger, J., & Tremblay, J.-É. (2022). Physical and Biogeochemical  
842 Influences on Nutrients Through the Canadian Arctic Archipelago: Insights from Nitrate  
843 Isotope Ratios. *Journal of Geophysical Research: Oceans*, n/a(n/a), e2021JC018179.  
844 <https://doi.org/10.1029/2021jc018179>
- 845 Letscher, R. T., Hansell, D. A., Kadko, D., & Bates, N. R. (2013). Dissolved organic nitrogen  
846 dynamics in the Arctic Ocean. *Marine Chemistry*, 148, 1–9.  
847 <https://doi.org/10.1016/j.marchem.2012.10.002>

- 848 Letscher, R. T., Hansell, D. A., Carlson, C. A., Lumpkin, R., & Knapp, A. N. (2013). Dissolved  
849 organic nitrogen in the global surface ocean: Distribution and fate. *Global Biogeochemical*  
850 *Cycles*, 27(1), 141–153. <https://doi.org/10.1029/2012gb004449>
- 851 Lewis KM, van Dijken GL, Arrigo KR. Changes in phytoplankton concentration now drive  
852 increased Arctic Ocean primary production. *Science*. 2020 Jul 10;369(6500):198-202. doi:  
853 10.1126/science.aay8380. Epub 2020 Jul 9. PMID: 32647002.
- 854 Link, P. M. & Tol, R. S. J. Economic impacts on key Barents Sea fisheries arising from changes  
855 in the strength of the Atlantic thermohaline circulation. *Global Environ Change* 19, 422–433  
856 (2009).
- 857 Lobbes, J. M., Fitznar, H. P., & Kattner, G. (2000). Biogeochemical characteristics of dissolved  
858 and particulate organic matter in Russian rivers entering the Arctic Ocean. *Geochimica et*  
859 *Cosmochimica Acta*, 26, 2973–2983.
- 860 Louiseize, N. L., Lafrenière, M. J., & Hastings, M. G. (2014). Stable isotopic evidence of  
861 enhanced export of microbially derived NO<sub>3</sub>- following active layer slope disturbance in the  
862 Canadian High Arctic. *Biogeochemistry*, 121(3), 565–580. [https://doi.org/10.1007/s10533-](https://doi.org/10.1007/s10533-014-0023-x)  
863 [014-0023-x](https://doi.org/10.1007/s10533-014-0023-x)
- 864 Manning, C. C. M., Preston, V. L., Jones, S. F., Michel, A. P. M., Nicholson, D. P., Duke, P. J.,  
865 et al. (2020). River Inflow Dominates Methane Emissions in an Arctic Coastal System.  
866 *Geophysical Research Letters*, 47(10). <https://doi.org/10.1029/2020gl087669>
- 867 McClelland, J. W., Holmes, R. M., Peterson, B. J., Raymond, P. A., Striegl, R. G., Zhulidov, A.  
868 V., et al. (2016). Particulate organic carbon and nitrogen export from major Arctic rivers.  
869 *Global Biogeochemical Cycles*, 30(5), 629–643. <https://doi.org/10.1002/2015gb005351>
- 870 McLaughlin, F. A., & Carmack, E. C. (2010). Deepening of the nutricline and chlorophyll  
871 maximum in the Canada Basin interior, 2003–2009. *Geophysical Research Letters*, 37(24).  
872 <https://doi.org/10.1029/2010gl045459>
- 873 Mellat, M. et al. Hydroclimatic Controls on the Isotopic ( $\delta^{18}\text{O}$ ,  $\delta^2\text{H}$ , d-excess) Traits of Pan-  
874 Arctic Summer Rainfall Events. *Frontiers Earth Sci* 9, 651731 (2021).
- 875 Peterson, B. J., Holmes, R. M., McClelland, J. W., Vörösmarty, C. J., Lammers, R. B.,  
876 Shiklomanov, A. I., et al. (2002). Increasing River Discharge to the Arctic Ocean. *Science*,  
877 298(5601), 2171–2173. <https://doi.org/10.1126/science.1077445>
- 878 Pfeffer, W. T., Arendt, A. A., Bliss, A., Bolch, T., Cogley, J. G., Gardner, A. S., et al. (2014).  
879 The Randolph Glacier Inventory: a globally complete inventory of glaciers. *Journal of*  
880 *Glaciology*, 60(221), 537–552. <https://doi.org/10.3189/2014jog13j176>
- 881 Rafter, P. A., DiFiore, P. J., & Sigman, D. M. (2013). Coupled nitrate nitrogen and oxygen  
882 isotopes and organic matter remineralization in the Southern and Pacific Oceans. *Journal of*  
883 *Geophysical Research: Oceans*, 118(10), 4781–4794. <https://doi.org/10.1002/jgrc.20316>
- 884 Rood, S. B., Kaluthota, S., Philipsen, L. J., Rood, N. J., & Zanewich, K. P. (2017). Increasing  
885 discharge from the Mackenzie River system to the Arctic Ocean. *Hydrological Processes*,  
886 31(1), 150–160. <https://doi.org/10.1002/hyp.10986>
- 887 Schlitzer, R. (2021). Ocean Data Viewer. Retrieved from <https://odv.awi.de>
- 888 Sigman, D. M., Casciotti, K. L., Andreani, M., Barford, C., Galanter, M. B. J. K., & Böhlke, J.  
889 K. (2001). A bacterial method for the nitrogen isotopic analysis of nitrate in seawater and  
890 freshwater. *Analytical chemistry*, 73(17), 4145–4153.
- 891 Sipler, R., & Bronk, D. (2014). Dynamics of Dissolved Organic Nitrogen. In D. A. Hansel & C.  
892 A. Carlson (Eds.), *Biogeochemistry of Dissolved Organic Matter* (Second, pp. 127–232).  
893 <https://doi.org/10.1016/b978-0-12-405940-5.00004-2>

- 894 Snyder, L., & Bowden, W. B. (2014). Nutrient dynamics in an oligotrophic arctic stream  
895 monitored in situ by wet chemistry methods. *Water Resources Research*, 50(3), 2039–2049.  
896 <https://doi.org/10.1002/2013wr014317>
- 897 Tang, C. C. L., Ross, C. K., Yao, T., Petrie, B., DeTracey, B. M., & Dunlap, E. (2004). The  
898 circulation, water masses and sea-ice of Baffin Bay. *Progress in Oceanography*, 63(4), 183–  
899 228. <https://doi.org/10.1016/j.pocean.2004.09.005>
- 900 Tank, S. E., Manizza, M., Holmes, R. M., McClelland, J. W., & Peterson, B. J. (2012). The  
901 Processing and Impact of Dissolved Riverine Nitrogen in the Arctic Ocean. *Estuaries and*  
902 *Coasts*, 35(2), 401–415. <https://doi.org/10.1007/s12237-011-9417-3>
- 903 Telling, J., Stibal, M., Anesio, A. M., Tranter, M., Nias, I., Cook, J., et al. (2012). Microbial  
904 nitrogen cycling on the Greenland Ice Sheet. *Biogeosciences*, 9(7), 2431–2442.  
905 <https://doi.org/10.5194/bg-9-2431-2012>
- 906 Terhaar, J., Lauerwald, R., Regnier, P. et al. Around one third of current Arctic Ocean primary  
907 production sustained by rivers and coastal erosion. *Nat Commun* 12, 169 (2021).  
908 <https://doi.org/10.1038/s41467-020-20470-z>
- 909 Thibodeau, B., Bauch, D., & Voss, M. (2017). Nitrogen dynamic in Eurasian coastal Arctic  
910 ecosystem: Insight from nitrogen isotope. *Global Biogeochemical Cycles*, 31(5), 836–849.  
911 <https://doi.org/10.1002/2016gb005593>
- 912 Treat, C. C., Wollheim, W. M., Varner, R. K. & Bowden, W. B. Longer thaw seasons increase  
913 nitrogen availability for leaching during fall in tundra soils. *Environ Res Lett* 11, 064013  
914 (2016).
- 915 Tremblay, J.-É., Raimbault, P., Garcia, N., Lansard, B., Babin, M., & Gagnon, J. (2014). Impact  
916 of river discharge, upwelling and vertical mixing on the nutrient loading and productivity of  
917 the Canadian Beaufort Shelf. *Biogeosciences*, 11(17), 4853–4868. [https://doi.org/10.5194/bg-](https://doi.org/10.5194/bg-11-4853-2014)  
918 [11-4853-2014](https://doi.org/10.5194/bg-11-4853-2014)
- 919 Tremblay, Jean-Éric, Michel, C., Hobson, K. A., Gosselin, M., & Price, N. M. (2006). Bloom  
920 dynamics in early opening waters of the Arctic Ocean. *Limnology and Oceanography*, 51(2),  
921 900–912. <https://doi.org/10.4319/lo.2006.51.2.0900>
- 922 Tremblay, Jean-Éric, Anderson, L. G., Matrai, P., Coupel, P., Bélanger, S., Michel, C., &  
923 Reigstad, M. (2015). Global and regional drivers of nutrient supply, primary production and  
924 CO<sub>2</sub> drawdown in the changing Arctic Ocean. *Progress in Oceanography*, 139, 171–196.  
925 <https://doi.org/10.1016/j.pocean.2015.08.009>
- 926 Vonk, J. E., Tank, S. E., Bowden, W. B., Laurion, I., Vincent, W. F., Alekseychik, P., et al.  
927 (2015). Reviews and syntheses: Effects of permafrost thaw on Arctic aquatic ecosystems.  
928 *Biogeosciences*, 12(23), 7129–7167. <https://doi.org/10.5194/bg-12-7129-2015>
- 929 Wadham, J. L., Hawkings, J., Telling, J., Chandler, D., Alcock, J., O'Donnell, E., et al. (2016).  
930 Sources, cycling and export of nitrogen on the Greenland Ice Sheet. *Biogeosciences*, 13(22),  
931 6339–6352. <https://doi.org/10.5194/bg-13-6339-2016>
- 932 Wagner, D., Spieck, E., Bock, E., & Pfeiffer, E.-M. (2002). Microbial Life in Terrestrial  
933 Permafrost: Methanogenesis and Nitrification in Gelisols as Potentials for Exobiological  
934 Process (p. 143). Berlin, Heidelberg: Springer Berlin Heidelberg. [https://doi.org/10.1007/978-](https://doi.org/10.1007/978-3-642-59381-9_10)  
935 [3-642-59381-9\\_10](https://doi.org/10.1007/978-3-642-59381-9_10)
- 936 Wang, X., & Veizer, J. (2000). Respiration–photosynthesis balance of terrestrial aquatic  
937 ecosystems, Ottawa area, Canada. *Geochimica et Cosmochimica Acta*, 64(22), 3775–3786.  
938 [https://doi.org/10.1016/s0016-7037\(00\)00477-4](https://doi.org/10.1016/s0016-7037(00)00477-4)

- 939 Wassmann, P., Duarte, C. M., Agusti, S., & Sejr, M. K. (2011). Footprints of climate change in  
940 the Arctic marine ecosystem. *Global Change Biology*, *17*(2), 1235–1249.  
941 <https://doi.org/10.1111/j.1365-2486.2010.02311.x>
- 942 Weigand, M. A., Foriel, J., Barnett, B., Oleynik, S., & Sigman, D. M. (2016). Updates to  
943 instrumentation and protocols for isotopic analysis of nitrate by the denitrifier method. *Rapid*  
944 *Communications in Mass Spectrometry*, *30*(12), 1365-1383.).
- 945 Wu, P., Wood, R., & Stott, P. (2005). Human influence on increasing Arctic river discharges.  
946 *Geophysical Research Letters*, *32*(2). <https://doi.org/10.1029/2004gl021570>
- 947 Wynn, P. M., Hodson, A. J., Heaton, T. H. E., & Chenery, S. R. (2007). Nitrate production  
948 beneath a High Arctic glacier, Svalbard. *Chemical Geology*, *244*(1–2), 88–102.  
949 <https://doi.org/10.1016/j.chemgeo.2007.06.008>
- 950 Yamamoto-Kawai, M., Carmack, E., & McLaughlin, F. (2006). Nitrogen balance and Arctic  
951 throughflow. *Nature*, *443*(7107), 43–43. <https://doi.org/10.1038/443043a>
- 952 Ye, F., Guo, W., Wei, G., & Jia, G. (2018). The Sources and Transformations of Dissolved  
953 Organic Matter in the Pearl River Estuary, China, as Revealed by Stable Isotopes. *Journal of*  
954 *Geophysical Research: Oceans*, *123*(9), 6893–6908. <https://doi.org/10.1029/2018jc014004>  
955

956 **Tables**957 **Table 1.** End member values used in the mixing model (from Yamamoto– Kawai et al., 2008  
958 and Alkire et al., 2010).

End Member	Salinity (PSU)	$\delta^{18}\text{O}\text{-H}_2\text{O}$ (‰)
Pacific Water	33	-0.80
Atlantic Water	35	0.20
Freshwater (rivers & glaciers)	0.0	-20
Sea Ice	4.0	0.05

959

960 **Table 2.** Concentration and  $\delta^{15}\text{N}$  and  $\delta^{18}\text{O}$  of  $\text{NO}_3^-$  and DON, as well as  $\Delta(15,18)$  of  $\text{NO}_3^-$  in  
961 river samples (calculated as in Rafter et al., 2013). “R” denotes rivers sampled. Rivers were  
962 named based on proximity to geographic features or CTD stations, and are named as follows:  
963 Devon Island West (R-DIW), Devon Island East (R-DIE), Copland Point (R-CP), Devon Island  
964 West North (R-RIWN), Sydkap Glacier (R-SG), Eastern Sydkap Icecap (R-ESC), Station 6.1 (R-  
965 6.1), Eugenie’s Sister Glacier (R-ESG), Station 135 (R-135), Ellesmere Island East (R-EE), and  
966 Hans Island (R-HI).  
967

STATION	$[\text{NO}_3^-]$	$\delta^{15}\text{N}\text{-NO}_3^-$	$\delta^{18}\text{O}\text{-NO}_3^-$	$\Delta(15,18)$	[DON]	$\delta^{15}\text{N}\text{-DON}$
<b>R-DIW</b>	20	4.4	-9.3	14	1.6	
<b>R-DIE</b>	1.3	3.4	18	-14	0.54	
<b>R-CP</b>	4.1	2.9	-7.5	10	2.2	
<b>R-DIW-N</b>	47	4.8	-9.6	14	0.99	
<b>R-SG</b>	2.7	0.71	-1.4	2.1	3.1	5.8
<b>R-ESC</b>	3.3	2.6	-6.3	8.9	1.8	
<b>R-6.1</b>	11	10	-2.7	13	0.0	
<b>R-ESG</b>	0.44	10	49	-38	4.9	7.2
<b>R-135</b>	3.5	6.6	7.3	-0.68	0.16	
<b>R-EE</b>	2.7	4.8	10	-5.4	1.5	
<b>R-HI</b>	4.7	5.3	-0.80	6.1	1.4	

968

969

970

971

972

973

974

975

976

977

978

979

980

981

982 **Figures**

983  
984  
985  
986  
987  
988  
989  
990  
991  
992  
993  
994  
995  
996  
997  
998  
999  
1000  
1001  
1002  
1003  
1004  
1005  
1006  
1007  
1008  
1009  
1010  
1011  
1012  
1013  
1014  
1015  
1016  
1017  
1018  
1019  
1020  
1021  
1022  
1023  
1024  
1025  
1026  
1027  
1028  
1029  
1030  
1031  
1032  
1033  
1034

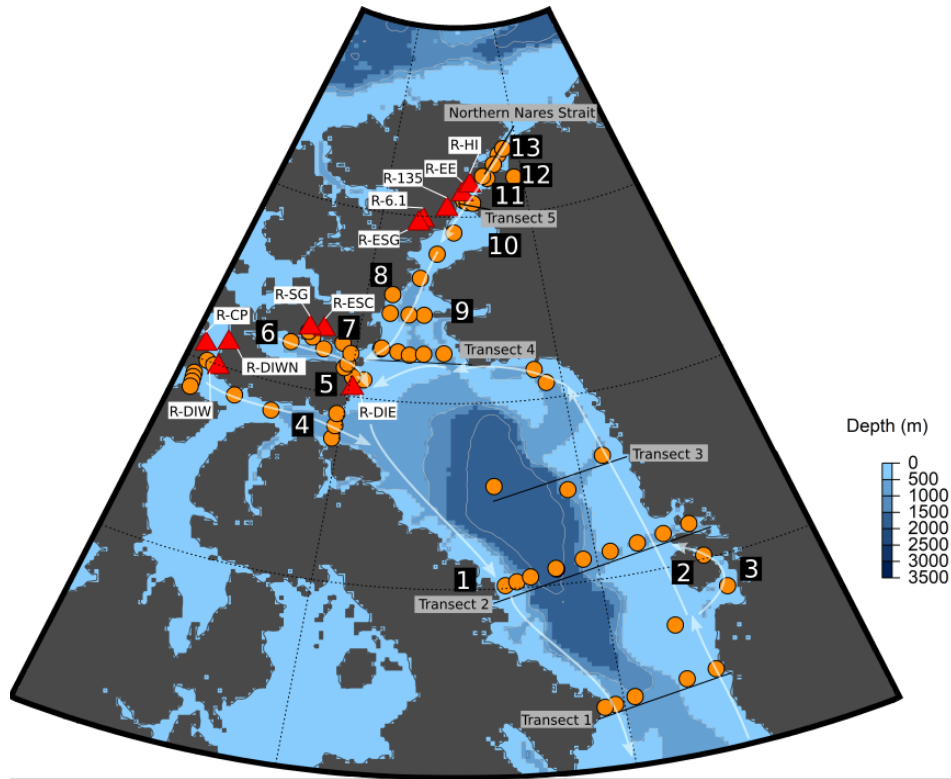


**Figure 1.** Map of the sampling locations. CTD casts are marked with orange circles. Red triangles represent river locations, which are also labeled by name. Transects 1, 2, 3, 4, 5, and the Northern Nares Strait are also labeled with solid black lines. The directions of surface currents are shown by the white arrows. Important regions and features numbered as follows: 1: Clyde River, 2: Disko Island, 3: Jakobshavn Glacier, 4: Lancaster Sound, 5: Devon Island, 6: Jones Sound, 7: Manson Icefield, 8: Talbot Inlet, 9: Smith Sound, 10: Kane Basin, 11: Kennedy Channel, 12: Petermann Glacier, 13: Hall Basin. 9–13 are all considered part of Nares Strait.

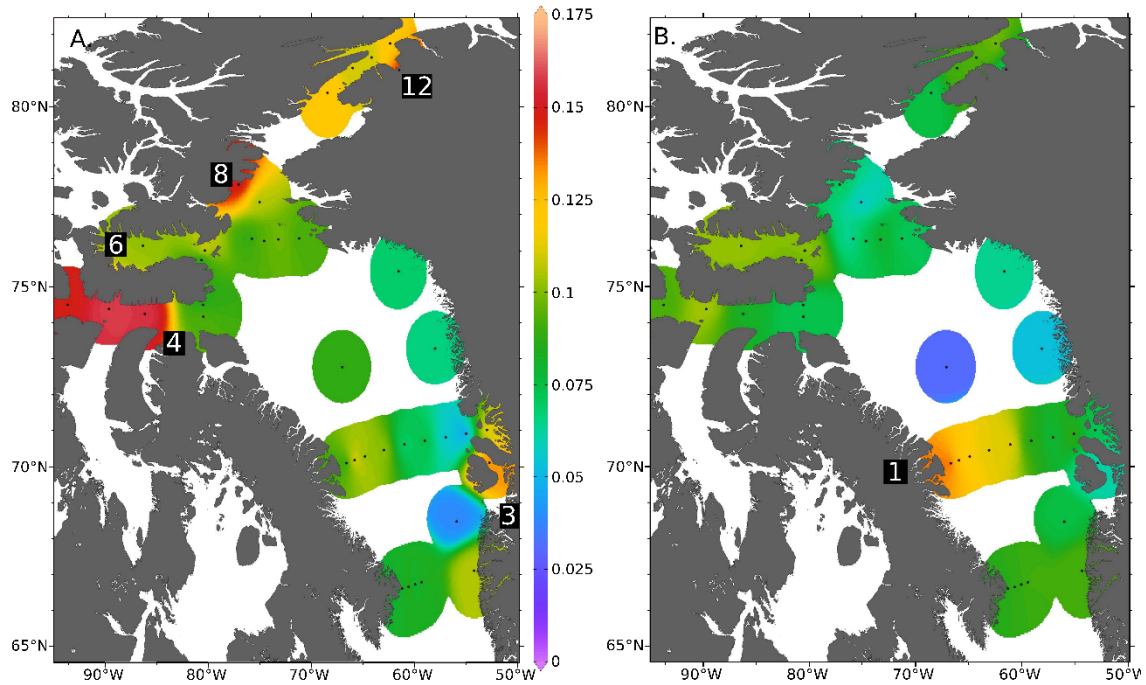


**Figure 2.** A. Fraction of freshwater and B. fraction of sea ice melt in surface water. 1- Clyde River, 3 – Jakobshavn Glacier, 4 – Lancaster Sound, 6 – Jones Sound, 8 – Talbot Inlet, 12 – Petermann Glacier.

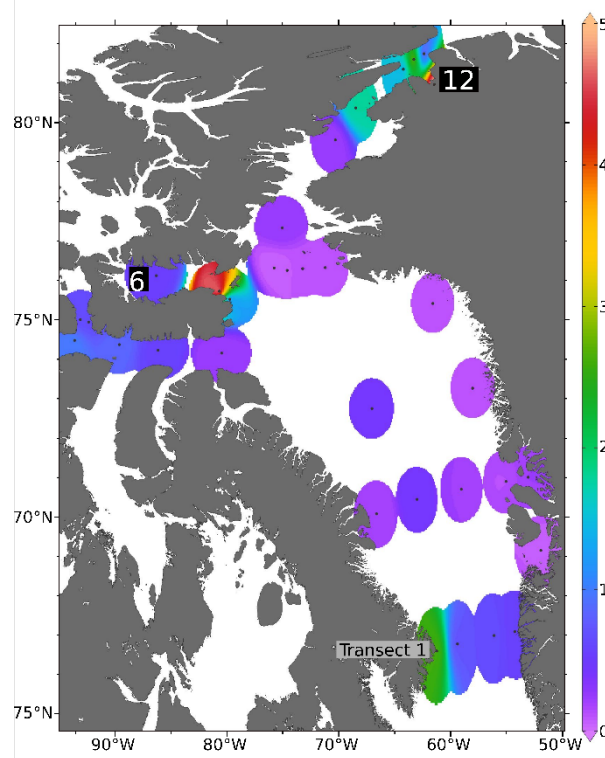


**Figure 3.** Surface chlorophyll-a ( $\mu\text{g L}^{-1}$ ), regions with blooms at Petermann Glacier (12), Jones Sound (6), and Western Transect 1

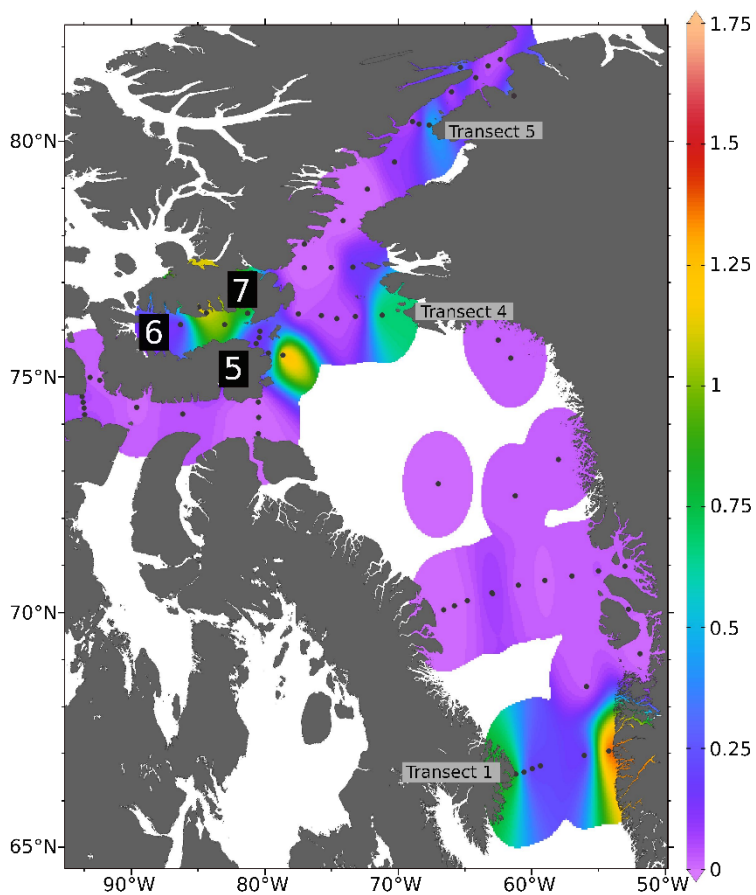


**Figure 4.**  $\text{NO}_3^-$  ( $\mu\text{M}$ ) distribution in the surface of the study area. Regions with measurable  $\text{NO}_3^-$  concentrations are labeled as in Figure 1.

1036  
1037  
1038  
1039  
1040  
1041  
1042  
1043  
1044  
1045  
1046  
1047  
1048  
1049  
1050  
1051  
1052  
1053  
1054  
1055  
1056

1057

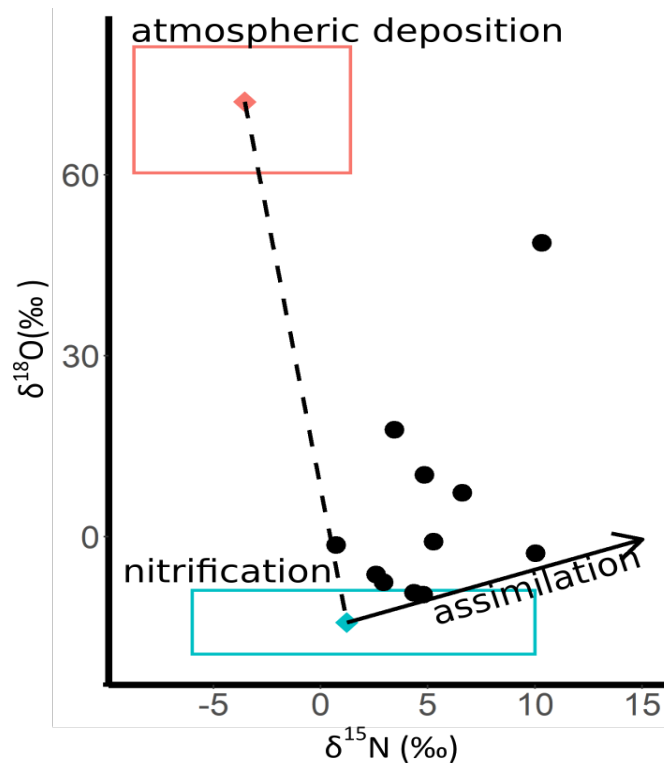
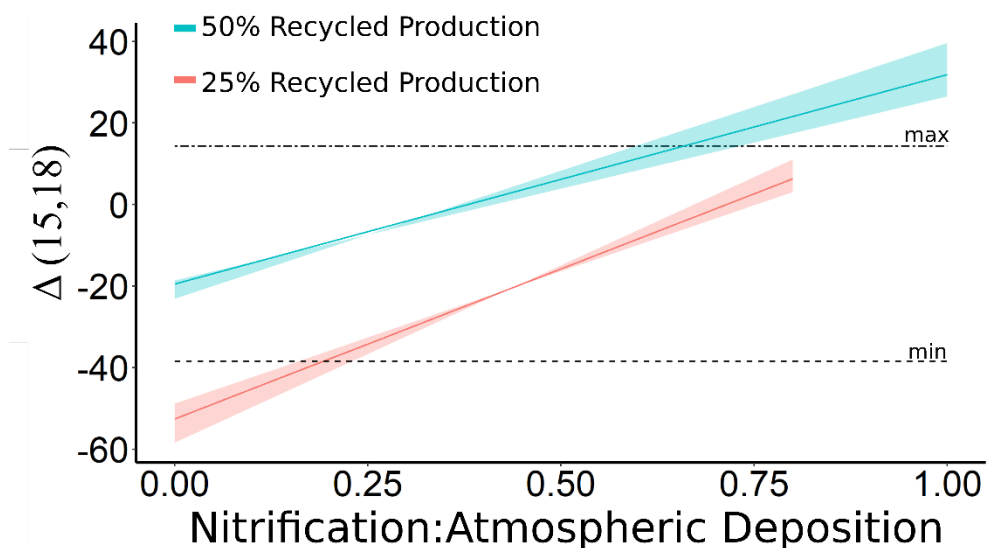


**Figure 5.**  $\delta^{18}\text{O}$  vs  $\delta^{15}\text{N}$  of  $\text{NO}_3^-$  for riverine samples, with mixing between nitrification of  $\text{NH}_4^+$  (blue box) and atmospheric deposition (pink box) marked by the dashed line. The  $\epsilon^{18}$ :  $\epsilon^{15}$  of assimilation ( $\sim 1$ ) is noted with the solid black arrow.

1058

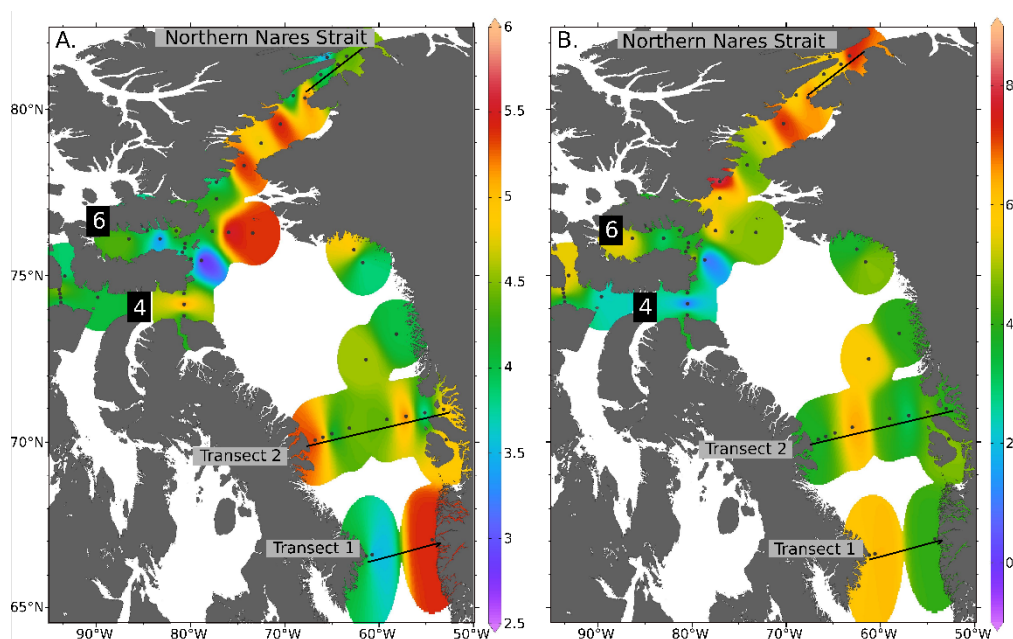
1059

1060



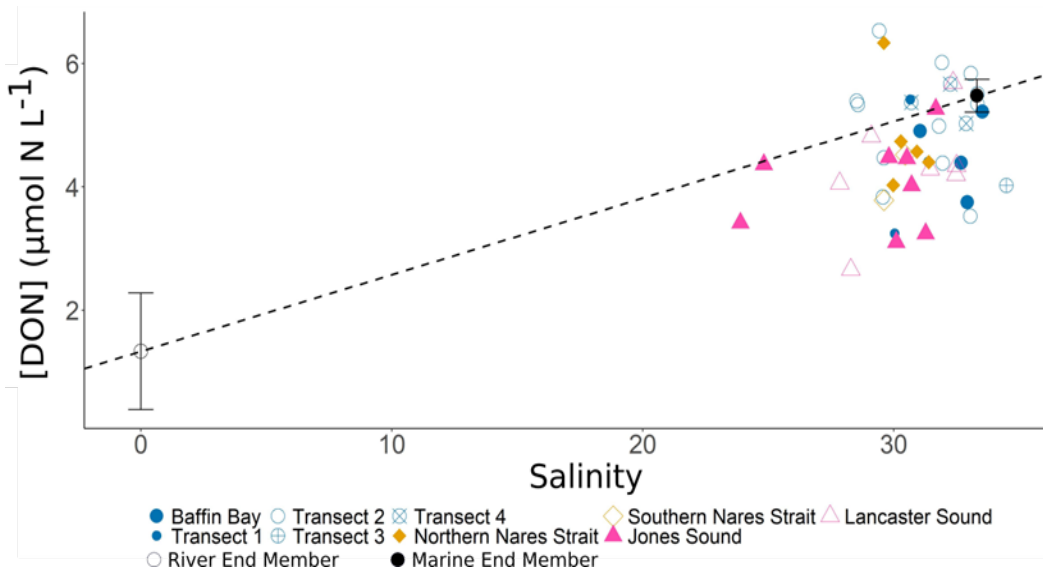
**Figure 6.** Results from simple box model simulations evaluating the capacity of different sources of  $\text{NO}_3^-$  in glacial rivers of the ECAA to generate  $\text{d}^{15}\text{N}$  and  $\text{d}^{18}\text{O}$  and  $\Delta(15,18)$  signatures. The ratio of nitrified  $\text{NH}_4^+$ : atmospheric deposition is on the x axis, and  $\Delta(15,18)$  on the y-axis. The blue line represents 50% recycled production, and the pink line represents 25% recycled production. The shaded colors represent model outputs when using the outer ranges of the end members. The black dashed lines represent the minimum and maximum  $\Delta(15,18)$  observed in riverine samples.

1061  
1062

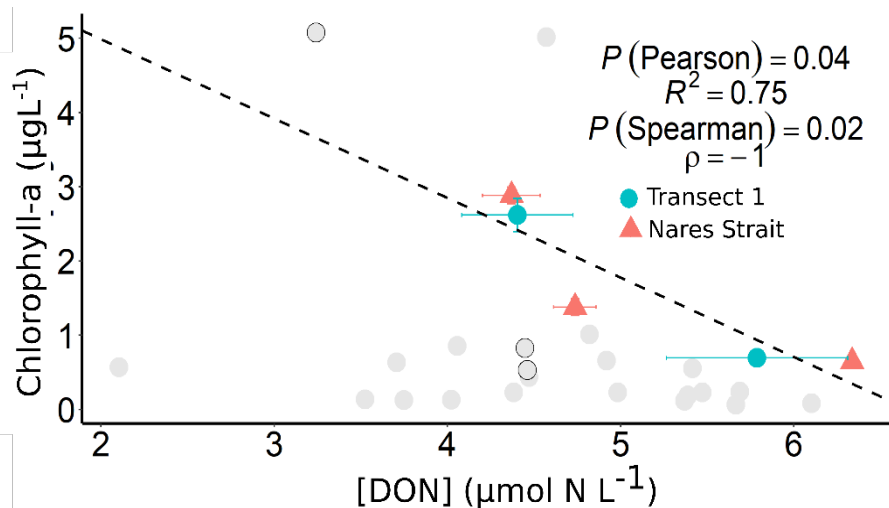


**Figure 7.** A.  $[\text{DON}]$  ( $\mu\text{M N L}^{-1}$ ) and B.  $\delta^{15}\text{N}$  of DON in the surface water. Transects 1, 2, and Northern Nares Strait are denoted with black text. Lancaster (4) and Jones (6) Sounds are also labeled.

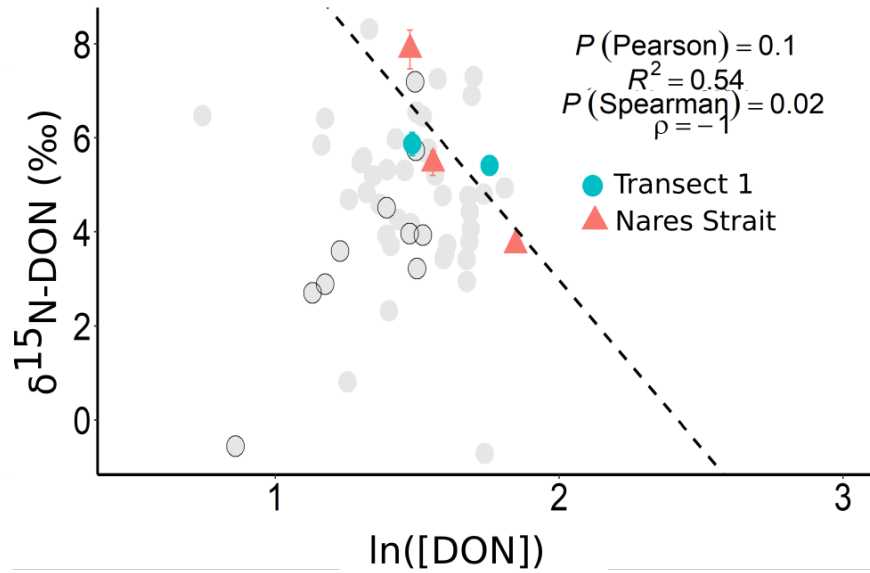
1063



**Figure 8.** [DON] ( $\mu\text{M N L}^{-1}$ ) in the mixed layer (upper 10 meters) of the water column vs salinity. Color indicates close geographic proximity: Blue dots represent samples located within Baffin Bay, orange diamonds represent samples in Nares Strait, and pink triangles represent samples located in sounds to the east of Baffin Bay. Riverine (hollow) and marine (solid) end members are marked with black dots with solid lines representing standard deviation in our estimates. The dashed line represents mixing between the two end members. Standard deviation  $< 0.5 \mu\text{M}$  for [DON].



**Figure 9.** Surface [DON] ( $\mu\text{M N L}^{-1}$ ) in the northern Nares Strait (north of  $80^\circ\text{N}$ ) (comprising Hall Basin and Kennedy Channel) and western Transect 1, against chlorophyll-a concentration ( $\mu\text{g L}^{-1}$ ). The Pearson and Spearman's rank correlation coefficients and p-values ( $P$ ) are shown. Data from all other stations are shown with light grey dots, with Jones sound outlined in black.

1064  
1065

**Figure 10.** Surface  $\ln$ (DON) vs  $\delta^{15}\text{N}$  of DON in the northern Nares Strait (north of  $80^\circ\text{N}$ ) and western Transect 1. The Pearson and Spearman's rank correlation coefficients and p-values ( $P$ ) are shown. Data from all other stations are shown with light grey dots, with Jones Sound outlined in black

1066  
1067  
1068